Graphene-Based Polymer Composites: Physical and Chemical Properties

Srikanta Moharana, Bibhuti B. Sahu, Lipsa Singh, and Ram Naresh Mahaling

Abstract The graphene-based polymer composites are of immense interest for their end-use applicability in the field of electromagnetic interference shielding devices, tissue engineering, sensor, power storage, supercapacitors, and energy storage devices. Graphene oxide is one of the finest nanomaterials with outstanding physical and chemical properties for the choice of scientific and engineering applications. The present chapter is focused mainly on two categories. In the first category synthesis technique is based on electrospinning for the fabrication of graphene-reinforced polymeric composites. In the second one, we have primarily emphasized graphene-based composites with many organic and polymeric materials including polyvinyl alcohol (PVA), poly(vinylidene fluoride) (PVDF), epoxy, polystyrene (PS), polypropylene (PP), polyimide (PI), polyurethane (PU), polyaniline (PANI), polypyrrole, and polythiophene in more detail. In addition, the thermal, mechanical, and electrical properties of these graphene-based polymeric composites have been discussed in a lucid manner. The concluding section of this current chapter throws light on the current challenges and opens the path for these new promising composite materials for their technological applications as per the contemporary demands.

Keywords Graphene · Polymer · Composites · Thermal properties · Dielectric properties · Energy storage

S. Moharana (✉) · L. Singh
School of Applied Sciences, Centurion University of Technology and Management, Bhubaneswar, Odisha, India

B. B. Sahu
Department of Physics, Veer Surendra Sai University of Technology, Burla, Odisha, India

R. N. Mahaling (✉)
Laboratory of Polymeric and Materials Chemistry, School of Chemistry, Sambalpur University, Jyoti Vihar, Burla, Odisha 768019, India
e-mail: rnmahaling@suniv.ac.in

S. Sahoo et al. (eds.), *Defect Engineering of Carbon Nanostructures*, Advances in Material Research and Technology, https://doi.org/10.1007/978-3-030-94375-2_7

1 Introduction

During the past decade, carbon-based polymer composite materials (graphene oxide) are of great importance for several strategic technologically advanced applications like electronic devices, electromagnetic interference shielding devices, tissue engineering, sensor, power storage, supercapacitors, etc. [1–5]. Recently, academic researchers have examined materials with enhanced properties of composite systems that are dimensionally more appropriate in the areas of modern science and technology and found carbon-based polymeric materials are of a wide range of potential applicability due to their structural characteristics. Typical carbon-based materials such as graphite, carbon nanotubes (CNTs), and graphene, in particular, have tremendous attention due to their excellent thermal, electrical, and mechanical performance. Graphite is considered to be the most crystalline form of the element in which carbon atoms are arranged in a hexagonal crystal structure [5–11]. However, the single-phase graphite (act as filler) cannot accomplish the high energy storage density while maintaining satisfactory dielectric and mechanical breakdown strength. As a result, small quantities of fillers are incorporated into the polymer matrix to constitute the graphite-based polymer composites [11–13]. These polymeric composites comprising graphene-based fillers have opened a scope of promising fields for material science and engineering due to their lightweight, easy processing, high specific strength, and exceptional dielectric and electrical performance [14, 15].

Graphene has attracted immense interest due to its extraordinary properties with respect to the combination of physics, chemistry, and materials science. Graphene is the most significant among the different members of the carbon family having sp^2 hybridized two-dimensional structures with honeycomb crystal lattice [16–18]. For instance, Geim et al. [17, 19] have successfully isolated single-layered transferable graphene nanosheets by using a peeling process involving the scotch tape method. These graphene-based composites have exceptional properties, including high current density, chemical inertness, high thermal conductivity, excellent optical transmittance, high carrier mobility, and high mechanical strength with superior Young's modulus. Initially, graphene was taken out from graphite using the micromechanical cleavage technique. This technique is usually used for easy production of high-quality graphene and to promote more experimental activities [19]. Further, the combination of graphene with polymer matrix composite is an excellent candidate for better electrical performance used as a sensor because of its 2D structure, which makes it very efficient to detect absorbed molecules. Besides, the high electrical conductivity and optical transparency of graphene support as superior candidates for end-use practical applicability in the field of conducting electrodes, touch screens, organic light-emitting diodes (OLEDs), and organic photovoltaic cells [20, 21].

Similarly, the Toyota research group [22] reported on the discovery of polymer-based composite, which gave a new dimension in the field of material science. Specifically, the inorganic filler-based composite materials (inorganic polymer) have attracted increasing attention due to their distinctive properties and wide potential applications in aerospace, automotive, construction, and electrical and electronic

industries [3–5, 20, 21]. Consequently, most academic and industrial researchers have developed polymer nanocomposites based on layered materials such as montmorillonite type [layered double hydroxide (LDH)]. The thermal and electrical conductivity of clay minerals is reasonably poor [23, 24]. Thus, to overcome these limitations, carbon-based materials such as carbon nanotubes (CNTs), carbon nanofibers (CNF), carbon black (CB), etc. have been incorporated into polymer matrix for preparing polymer composites [25–28]. In the previous literatures, it has been reported that carbon nanotubes (CNTs) are especially used as conductive fillers (nanofillers) but their production cost is high [25–30]. So it is very difficult for mass production of CNT-based functional composite materials. Interestingly, graphene has been chosen as alternative nanofillers to overcome the limitations of conventional nanofillers (Na-MMT, LDH, CNT, CNF, etc.) due to high surface area, aspect ratio, good flexibility, thermal and electrical conductivity, and low-cost production [23–31].

The significant performances of graphene compared to the neat polymer are remarkable when it becomes polymer-filled graphene composites. Polymer-based graphene nanocomposites exhibit better mechanical, electrical, gas barrier, thermal, and flame-retardant properties with respect to pristine polymer matrix. However, it has been reported that the enhancement of electrical and mechanical behavior of graphene-based polymer composites is much superior to that of other carbon filler-based polymer nanocomposites [6–11, 32]. These enhancements in the behavior of resultant composites depend on the distribution of graphene layers in the polymer matrix as well as interfacial bonding between the graphene layers and polymer matrices. This interfacial interaction between graphene and pristine polymer may give rise to the final properties of the graphene-reinforced polymer nanocomposites. However, pure graphene is not compatible with organic polymers and also exhibits in-homogeneity in the composites. On the other hand, graphene oxide surface shows various kinds of oxygen-containing functional groups (including hydroxyl, epoxy, carboxyl, etc.) that alter the van der Waals interaction considerably, which makes good compatibility with organic polymeric materials [33–36]. In addition, there are some additional carbonyl and carboxyl functional groups placed in the sheets, resulting in strong hydrophilic graphene oxide, which readily swells and disperses in water. Therefore, graphene oxide has drawn considerable interest as nanofillers for polymer nanocomposites [21]. The graphene oxide sheets are commonly dispersed in aqueous media, which are incompatible with the organic polymers. Thus, graphene and graphene oxides are electrically insulating, which are incompatible with the fabrication of conducting polymer-based composites [37]. Further, surface modification is the crucial aspect for the improvement of the physical and chemical properties as well as a molecular level of distribution, which have a positive influence on the application of graphene reinforcing polymers. As a result, it is of enormous significance to fabricate polymer–graphene nanocomposites with improved strength and toughness simultaneously.

Because of scientific interest and potential applications of graphene-based polymer composite, research has been increased to a surprising dimension, opening new challenges and opportunities for better performance as well as end-use practical

applicability in the various technological fields. This typical chapter is mainly divided into two categories. The first one is particularly focused on the electrospinning technique of graphene–polymer composites; on the other hand, the second one covers properties and its various polymer-based graphene composites for energy storage and various important applications. Finally, a conclusion has been drawn on this new and exciting field of research of graphene-based polymer composites, followed by summary and perspective.

2 Synthesis of Graphene-Based Polymer Composites

2.1 Electrospinning Technique

Electrospinning technique is a simple, straightforward, and versatile method to synthesize one-dimensional (1D nanofibers) and two-dimensional (2D, nanowoven fabric) nanostructured materials [38–43]. Moreover, it is a multipurpose synthesis method for the fabrication of polymer nanofibers with precise diameter in the region of nanometers to micrometers [44]. There are various electrospun functional polymer nanofibers that can be reinforced with carbon-based materials, including CNTs, graphenes, nanodiamonds, nanodots, etc., which can significantly improve the properties (thermal, mechanical, dielectric, and electrical) of the composites and also leads to the potential applications, especially in the field of biology and sensors [38–44]. Among various methods of synthesis, electrospinning is a well-established technique for the fabrication of nanosized polymer fiber-based materials [44]. This technique has earned popularity due to its simplicity and implementation in diverse areas of tissue engineering, chemical and biological sensing, and energy sectors. The concept of electrospinning was observed from the study of electrospraying technique by Rayleigh and Zeleny in the last century [45]. Before a couple of decades, the term electrospinning was coined, due to its versatility and easy processability; this technique was rapidly established in different fields. Moreover, with due course of time, it is upgraded and modified for effective mass production of nanosized fibers. Scientists have tried to improve the physicochemical properties of electrospun material. Poly(sulfone amide) (PSA) has been used as a spinnable polymer recognized for its exceptional thermal properties (heat resistance, flame retardant, thermal stability, etc.). Moreover, it is also used for developing products for protective use in aerospace, high-temperature environment, and civil fields [46, 47]. The electrospun PSA nanofiber is unique for retaining superior performances in terms of crystallization, thermal and mechanical properties, and its nanostructure [48]. There are various advanced techniques relating to electrospinning, like coaxial electrospinning, mixed and multilayer electrospinning, forced air-assisted electrospinning, and air gap electrospinning, which have emerged for enhancing the properties of electrospun-nanosized fibers [49]. The main components of electrospinning processing setup comprise a high-voltage power supply, spinneret (commonly blunt

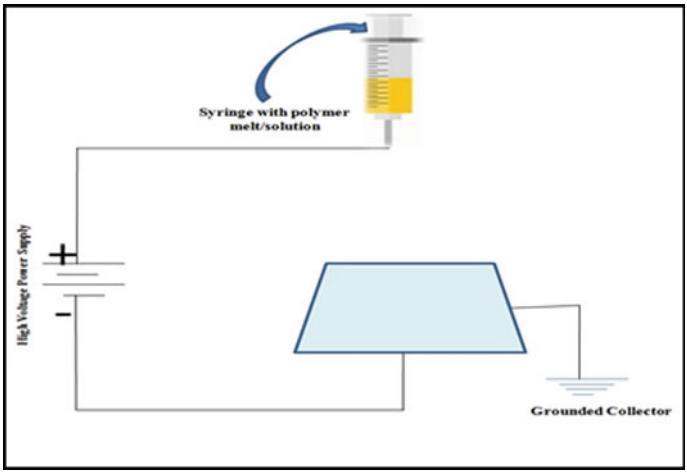

Fig. 1 Electrospinning experimental setup

needled syringe), and grounded collector. This unique technique for manufacturing continuous fiber from polymer melt/solution follows the principle of surface tension acting on polymer drops. The basic process of production is first initiated by placing the solution into the syringe held by a retort stand or by a syringe pump. Then the tip of the needle of the syringe is connected with a positive terminal of the voltage supply. Out of which, the polymer liquid is pumped by the needle to the collector (basically grounded) below the syringe [50]. The experimental setup is shown in Fig. 1.

There are various studies available based on graphene-based polymer composites by using electrospinning technique reported by several researchers. For instance, Bao et al. [51] have successfully prepared electrospun nanocomposites comprising polyvinyl acetate and graphene oxide (GO) and significant enhancement in optical properties was observed. Das et al. [52] have reported on loading of electrospun nanofibers on functionalized graphene for increasing crystallinity and superior thermal stability. Kim et al. [53] have been successful in synthesizing silica-encapsulated carbon nanofiber composites from a graphene–polyacrylonitrile (PAN) solution by the application of electrospinning technique. Further, using electrospinning nylon-6 shows interesting modified physical properties as well as fiber morphology because of polyelectrolytic and polymorphic nature [53]. Correa et al. [54] have fabricated rGO-polycaprolactone (PCL) composites with various weight percentages of rGO contents (0.25, 0.5, 0.75, and 1 wt%) by using electrospinning technique. In this composite system, two different voltage setups (10 and 15 kV) and distance of 10 cm are commonly used for electrospinning. The thermal, mechanical, microstructure, electrical, porosity, and absorption water analysis of the rGO-PCL composites were also made to the scaffold. However, a nanocomposite with electrospun at 10 kV exhibits enhancement of mechanical performance with an increase in the 190% of Young's modulus than that of the nanocomposites without rGO. On the

other hand, the samples of electrospun at 15 kV signify deterioration with the incorporation of rGO but simultaneously increase the electrical conductivity and porosity. Besides, the incorporation of 0.75 and 1 wt% of rGO-reinforced PCL nanocomposite shows detriment on properties, which may be attributed to the formation of aggregation of particles into the polymer matrix. Further, the effect of voltage on the electrospinning technique plays a significant contribution toward the final properties of the rGO-reinforced PCL nanocomposites. Guo et al. [55] reported that the thermally conductive CMG-polyimide nanocomposites by using in situ polymerization and electrospinning hot press technique. In these nanocomposites, the NH_2-modified POSS molecules are successfully grafted on the surface of GO and CMG through a reaction between NH_2-POSS and GO. However, the coefficient of thermal conductivity (I), heat resistance index (THRI), and glass transition temperature (Tg) of the synthesized CMG-PI nanocomposites with 5 wt% of CMG was significantly enhanced to 1.05 Wm^{-1} K^{-1}, which is about four times larger than that of the neat PI matrix (0.28 Wm^{-1} K^{-1}). Further, the Tg and THRI values simultaneously improved to 213.0 °C and 282.31 °C, respectively. An enhanced thermal conductivity model was also suggested that predicted the value of coefficient of thermal conductivity in the resultant nanocomposites, which is more accurately calculated than that of the typical Maxwell, Russell, and Bruggemen classical models. Hou et al. [56] have prepared homogeneous polyamide 6 (PA6)-graphene-based nanocomposite fibers using melt spinning and drawing process. It is observed that the resultant nanocomposites, graphene sheets are well dispersed within the matrix uniformly and also increased physio-mechanical performance of the nanocomposites. The graphene was oxidized to form graphene oxide, which is then reacted with amine compound to form the graphene bonding with amine functional groups and simultaneously synthesized nanocomposite fibers. The presence of PA6 on the surface of the graphene sheet is confirmed by FTIR, TGA, and AFM analysis. Moreover, 0.1 wt% of graphene content in the nanocomposites exhibited enhanced tensile strength with an increase in the graphene loading, which is much higher than that of the pristine polymer matrix. Roostaie et al. [57] synthesized polyamide–graphene oxide nanocomposites via electrospinning technique through stainless steel wire as a robust substrate. The nanocomposites with high porosity and diameter in the range of 100–250 nm were produced, which is confirmed by using scanning electron microscopy. However, the polyamide–graphene nanocomposite is fast and sensitive that offers sub (2–5 mg L^{-1}) and low ppt detection limits (0.7–1 mg L^{-1}) at an equilibrium time of about 15 min. This technique was applied to real water samples and relative recoveries in the range of 89–101% are obtained, which is no matrix effect. Similarly, Karumuthil et al. [58] have reported electrospun poly(vinylidene fluoride-trifluoroethylene)-based zinc oxide and exfoliated graphene oxide nanocomposite fibers for the applicability in the field of piezoelectric nanogenerators via electrospinning technique. These nanocomposites show superior energy generation efficiency and potential material for energy harvesting applications. Further, the synthesized nanocomposites were characterized by scanning electron microscopy, Fourier-transform infrared spectroscopy, and X-ray diffraction technique.

2.2 Dip Coating Technique

Dip coating method is commonly utilized for the preparation of graphene-based composites when a liquid polymer is used as a matrix. In this technique, initially neat graphene foam is incorporated into the polymer solution with varying dipping time which determines the quality and formation of coating and composites. However, the curing of polymer–graphene system takes place under suitable time and temperature conditions after completing the dip coating. Various researchers have fabricated graphene-based polymer composites via dip coating technique. Neito et al. [59] synthesized graphene foam (GrF)-doped polylactic acid-poly-e-caprolactone copolymer (PCL) hybrid scaffold with an attractive performance of graphene including excellent structural properties and enables retention of the porous 3D networked structure. However, the outstanding wettability of graphene foam-doped PLC scaffold showed improved strength (≈3700%) and increased ductility (≈3100%). Samad et al. [60] have fabricated free-standing graphene foam (GF) using three different processing techniques, including vacuum-assisted dip-coating of nickel foam (Ni-F) with graphene oxide (GO), reduction of GO to reduced graphene oxide (rGO), and etching out the nickel scaffold. It is observed that neat GF was examined by using microstructure, chemistry, and mechanical integrity. The microstructure of the GF mimics with Ni-F, as individual bones of GF were hollow, due to the entire removal of nickel. Moreover, PDMS-GF composites were characterized by their ability to sense both compressive and bending strains with varied electrical resistance. Sun et al. [61] have prepared reduced graphene oxide (rGO) through dip coating method by using graphene oxide suspension followed by thermal annealing. The growth of GO in this technique was tested through UV–Vis, microstructure, and the structure of the neat GO films via AFM, SEM, and XPS. They revealed that GO films can grow uniform thickness on the surface of the quartz slides and a controlled microstructure of the resultant films by coating cycles and content of solid GO suspension. The best quality of rGO film was achieved when the content of solid GO suspension (0.3 mg mL^{-1}) with five coating cycles followed by annealing at 600 °C in Ar/H_2 atmosphere. The sheet resistance (60 kV%21) and the transmittance (81%) at 550 nm may be a talented approach for synthesizing neat rGO films or composite films. Cheng et al. [62] have reported highly conductive multifunctional graphene-coated glass fiber with elevated electrical conductivity via sol–gel and dip coating technique. These graphene-based glass fibers have better electrical conductivity (24.9 S/cm) than that of the nanocarbon-coated fiber and commercial carbon fiber. The properties of wettability and electrical conductivity of the coated glass fibers are strongly dependent on the dip coating times and coating thickness in association with the coverage degree and compact structure of the graphene coatings. This high conductivity of graphene-coated glass fibers has an enormous interest in the field of flexible conductive wires, highly sensitive sensors, and multifunctional fibers. However, dip coating method is effective for producing very thin membrane and useful for some properties like high adhesion as well as reproducibility. Chatterjee et al. [63] have reported that cotton-woven and knitted fabrics have electrical

conductivity along with the various concentration of graphene oxide as well as the number of coating cycles. The increase in the number of reduced graphene oxide sheets is due to an increase in coats. In a reduced graphene oxide mixture, silk fabric was dipped frequently [64]. From some studies, it has been reported that graphene composites and electrical heat elements were dip-coated on non-woven fabrics [65, 66]. Preparation of high-quality graphene oxide nanocomposites was occurred by vacuum dip coating method exhibiting flux of molecular sieves mechanism, which was dependent upon temperature and pressure. To get various concentrations of graphene oxide sol on the modified γ-alumina support, the graphene oxide membrane layer was prepared by vacuum dip coating method. Dip coating procedure is exhibited in four steps. The first step is the immersion speed of the sample holder. To prevent the substrate blade from removing the graphene on the dispersion surface, it is necessary to control the immersion speed. In the second step, it exhibits the substrate's immersion time inside the dispersion. In other words, the adherence of some graphene occurred on the substrate surface. The third step is the removal speed of the substrate which is a parameter to control the deposition of graphene on the top layer of the multilayered graphene.

2.3 Solution Casting Technique

Solution casting method is the fabrication method commonly used for the preparation of graphene-based composites. In this method, graphene foam is completely infiltrated with the solution of polymer. The mold containing graphene is filled with polymer. In mold comprising graphene, the polymer is poured. The nodes and branches of the graphene are coated by the polymer which goes through the pore deeply. In the presence of heat, polymerization of polymer containing the embedded graphene occur and in this way, graphene-based polymer composites are formed. Various researchers have fabricated graphene-based polymer composites via solution casting technique. Thomas et al. [67] reported the effect of neat graphene which is incorporated into nitrile rubber matrix by green approach as well as two different routes of fabrication such as latex casting and dry rubber mixing. By planetary ball milling process, accomplishments of pristine few layers graphene occurred and by using X-ray diffraction, Raman spectroscopy, and transmission electron microscopy analysis, it was characterized. Then the incorporation of that produced graphene as well as that multiwalled carbon nanotubes occurred into nitrile rubber latex separately. Bahrami et al. [68] reported that by using electrospinning and solvent casting method, polyurethane-graphene is fabricated as membranes. Characterization of such membrane occurs due to some properties like electrical, mechanical, physiochemical as well as biological properties. The electrospun mats have significantly higher electro conductivity than the casting films. Electro conductivity of the composites is improved due to the graphene which acts as an electrical bridge. The mats have higher mechanical properties as compared to that of film and it is improved by increasing the concentration of graphene up to 5 wt% and then reduction occurred. Dispersion of all

exfoliated graphene occurred in polyvinyl alcohol by using the solution casting technique. Polyvinyl alcohol is highly soluble in water due to the presence of hydroxyl groups in it [69]. The polymer electrolytes are prepared by the simple solution casting method. For better solubility of graphene oxide, acetone as well as 1-methyl-2-pyrrolidinone (NMP) act as a solvent in the ratio (40:60) [70, 71]. In this solvent, poly(vinylidene fluoride-co-hexafluoropropylene) PVdF-HFP having 50 wt% was dissolved and stirred for 12 h. Later, the addition of the plasticizer ethylene carbonate having 35 wt% has been done and stirred again for 2 h. Finally, the addition of ionic salt $LiClO_4$ (15 wt%) was performed to that above mixed solution and stirred for about 3 h. Then, on a glass petri dish, the final solution was casted and kept at 80 °C in the hot air oven for 24 h. Then, the membrane is exfoliated from the petri dish after keeping the membrane in a vacuum oven at a pressure of 400 mbar and 80 °C for 2 h. Yang et al. [72] reported that by solution casting method, 1 wt% graphene-oxide-doped poly(vinylidene fluoride-co-hexafluoropropylene)/EMIMBF4 ion gel polymer electrolyte was prepared for supercapacitor application. Fattah et al. [73] reported that by using solution casting method, one can prepare 2–8 wt% of graphite-oxide-doped poly(vinylidene fluoride-co-hexafluoropropylene)-EMI-BTI for the application of electron double-layer capacitor.

2.4 Spray Deposition Technique

Spray deposition method is used for the preparation of graphene-based composites in which electrostatic spray is used sometimes for the deposition of polymer matrix in the form of powder on graphene foam and thus, graphene foam-based polymer composites are formed. Various researchers have fabricated graphene-based composites via spray deposition method. Mohammed et al. [74] reported that polyaniline-graphite nanofiber nanocomposites can be prepared by spray-coated single-mode fiber sensor at room temperature. The ratio of polyaniline/graphite nanofiber nanocomposites polymer film is about 2:1. By differing the diameter of waist single-mode fiber which is spray-coated with polyaniline/graphite nanofiber, a comprehensive investigation in which polyaniline/graphite nanofiber nanocomposites-coated single-mode fiber, as well as etched-tapered single-mode fiber sensor, was performed at room temperature. Soltani et al. [75] reported that by using conventional as well as substrate vibration-assisted ultrasonic spray coating, a highly conductive transparent graphene-doped PEDOT:PSS composites thin film can be fabricated. Liquid droplets of a precursor can be controlled by electrostatic spray deposition method by applying electrostatic force at bank as well as microscale droplet size [76, 77]. Deposition parameters controlled droplet properties such as size and charges as well as the flow rate of the precursor and the voltage applied between the nozzle and substrate. Deposition method is more efficient as compared to uncharged droplet method. Due to more effectiveness, in the deposition method, the electric field controlled the motion of the droplet [76]. The standard of the film was influenced by the size of the

particles as well as the dispersal mechanism [76, 77]. The electrostatic spray deposition method plays a major role in various applications. Preparation of the reduced graphite oxide thin films was done via the electrostatic spray deposition method. This approach consists of a syringe pump used to feed the solution of precursors through a nozzle and thus fine droplets were produced after applying DC high-voltage power which was used for the biasing of the precursor solution. Adelowo et al. [78] have reported the applications of lithium-ion capacitor by using reduced graphene oxide which is sprayed as electrodes. In the electrostatic spray deposition method, reduced graphene oxide films were synthesized with the substrate's area of about 50 × 50 mm^2. The pros of this method are to synthesize thin film at ambient temperature which is a simple process rather. Moreover, the time of deposition controls the thickness of the film and in the presence of substrate temperature, graphene oxide can be reduced. Thus, the electrostatic spray deposition method is the candidate for the fabrication of reduced graphite oxide thin films in a large area. By using electrostatic spray deposition technique, fabrication of acetone gas sensor was done which is based on reduced graphene oxide film in order to signify the preparation of electronic devices.

2.5 Melt Mixing Technique

Melt mixing process is utilized for the preparation of graphene-based composites in which nanofiller is combined with polymer melt physically. This method is cost-effective, more versatile as well as environment-friendly. Thermoplastic polymers are widely utilized in this technique at elevated temperatures. In this method, there is no requirement of any solvent. Mixing of polymer matrix with graphene or its derivatives occurred in the molten state. By using a conventional method such as extrusion as well as injection molding, mixing of graphene or its derivative occurred mechanically with thermoplastic polymer at elevated temperature. Due to the cost-effectiveness, there can be some possibilities of producing large quantities of materials. In this technique, there is no involvement of any additive, compounds, or chemicals within the mixing unit. Various researchers have fabricated graphene-based polymer composites via the melt mixing process. Adak et al. [79] reported that polyurethane-functionalized graphene nanocomposites films can be synthesized using solution master batching and melt mixing process and then by compression molding. In polyurethane matrix, graphene sheets can be exfoliated partially and it is uniformly dispersed due to differing in the concentration of graphene which is about 0–3 wt%. Consequently, with an increase in concentration of graphene, there can be some improvement in the helium gas barrier of nanocomposites film, which shows the reduction in gas permeability of about 30% at 3 wt% graphene loading. The increase in the concentration of graphene significantly increases the stiffness as well as the tensile strength of the nanocomposites. To accelerate artificial weathering conditions up to 300 h, the prepared functionalized graphene nanocomposites film was exhibited. Nordin et al. [80] have reported that poly(lactic acid)/thermoplastic polyurethane graphene composites can be synthesized by using melt mixing process. By using a resistance

meter, electrical conductivity was tested and it is observed that in the presence of graphene nanoplatelets the resistivity of composite started to percolate. The threshold change in percolation is due to a change in blend composition, and by this, it is shown that the lowest threshold per location was observed at poly(lactic acid) 90/thermoplastic polyurethane 10 (PLA 90/TPU 10) blends. By calculating wetting coefficient along with Owen as well as Wendt equation, it was predicted that graphene nanoplatelet can be localized in poly(lactic acid)/thermoplastic polyurethane blend, and according to the prediction, it is observed that graphene nanoplatelet is present preferentially in thermoplastic polyurethane phase. The increase in thermoplastic polyurethane content leads to an increase in the elongation at break of the composites. The blending of elongation at break occurred after the addition of graphene nanoplatelet in poly(lactic acid) 50/thermoplastic polyurethane 50 blend. Noorunnisa et al. [81] reported that the linear low-density polyethylene and graphene nanoplatelet composites can be fabricated by using twin-screw extruder under various extrusion conditions. The electrical, mechanical as well as thermal properties may alter the screw speed, feeder speed as well as graphene nanoplatelet content. Thermal stability as well as conductivity improved by 2.7% and 43%, respectively, which is caused by the inclusion of graphene nanoplatelets in the matrix. Due to high thermal stability of the graphene nanoplatelets as well as the production of photon and charge carrier network in the matrix of polymer, some improvement in case of electrical conductivity from 10^{-11} to 10^{-5} S/m at 150 rpm may be observed.

3 Defects of Graphene

Recently, in nanotechnology, graphene and graphene-based polymeric composite materials are the most promising candidates. Although they have immense potential applications in the field of energy storage, electronics and optoelectronic devices, biosensors and gas sensors, etc., still it is very difficult to fabricate defect-free materials. So, it is very crucial for understanding and to differentiate between various defects types as well as the influence in the alteration in basic electronic properties of these composite systems. There are natural imperfections, and defects due to growth are generally observed in the structural defects [82–84] that deteriorate graphene-based device performances. Moreover, defects are introduced for getting better ideas about phenomena related to graphene. Whenever crystalline order is disturbed without the presence of any alien atom the defects in three-dimensional crystals are known as intrinsic defects. Various intrinsic defects sometimes lead to interesting effects and potential applications as well, which are observed like point defects, cluster defects, and boundaries/edges defects responsible for reducing the crystal symmetry [85–87]. However, extrinsic defects deal with the introduction of impurities or foreign atoms into the crystalline order. Stone et al. reported on point defects (Stone Wales defect) that the graphene lattice has a tendency to reconstruct the non-hexagonal rings without involving the removed or added atoms produce two pentagons and heptagons each with the rotation of any one of the C–C bonds through

90° [88]. Meyer et al. [89] reported on the single vacancies in graphene which is the simplest defect and had been observed also in the TEM image and the defect of the missed lattice point atom can be shown in Fig. 2. The single vacancies undergo the Jahn–Teller distortion due to the saturation of two of the three sagging bonds in the direction of the missing atom which results in the formation of a five and nine-membered ring.

Moreover, double vacancies occur by either combination of two SVs or by the removal of two neighboring atoms. There is no sagging bond present in a fully reconstructed DV so that two pentagons and one octagon appeared instead of four hexagons in perfect graphene, as shown in Fig. 3 [90]. Also, the atomic network becomes coherent with slight agitation in the bond lengths around the defect [89].

Defects at the boundaries/edges of graphene result due to local changes, i.e., continuous removal of carbon atoms from the boundaries which can be done by sputtering edge atoms with electrons with energies lower than the threshold energy for displacing atoms from a perfect graphene. Under these conditions, armchair edges

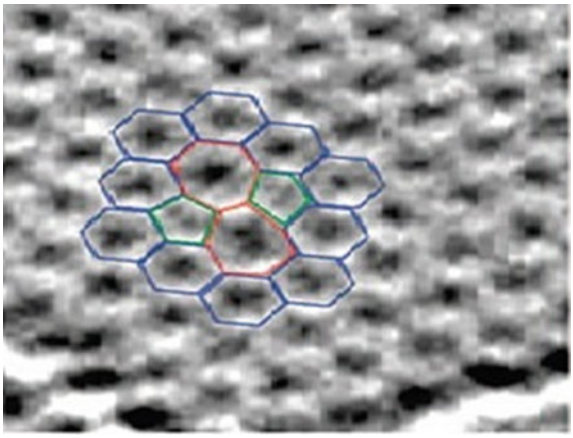

Fig. 2 Single-vacancy (SVs) TEM image of the defect in graphene (reprinted with permission from Ref. [89])

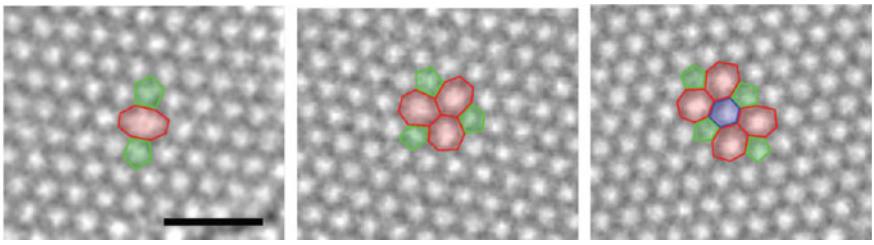

Fig. 3 Double vacancy (DV) TEM image of the defect in graphene (reprinted with permission from Ref. [90])

can be transformed to crisscross edges. An intermediate structure can be considered as a defective edge [91]. The removal of one carbon atom from a crisscross boundary leads to one pentagon in the middle of a row of hexagons at the edge. On the other hand, edge reconstructions result in different combinations of pentagons and heptagons at the boundaries. Banhart has reported on Foreign Adatom that if a non-carbon atom is there in graphene, it influences the properties of the graphene which is purely dependent on bonding with the foreign atom [92]. If the corresponding bond is weaker then due to van der Waals interaction physisorption occurs but the existence of stronger covalent bond results in chemisorptions.

3.1 Techniques for Creation of Defects

Generally, there are three techniques by which the non-equilibrium defects in graphene can be resulted such as particle irradiation, crystal growth, and chemical methods.

3.1.1 Particle Irradiation

The point defects can be obtained by irradiation of graphene, maybe with electrons/ions, as a result of ballistic expulsion of carbon atom [93], and threshold energy (~18–20 eV) has to be provided to abscond from its lattice site. Moreover, the atom may be then engrossed on the graphene expanse and drift on the surface as Adatom or stammer away from graphene. Ion irradiation is another physical method basically employed for producing defects in graphene [94], where several SVs and DVs are graphene-irradiated by using different noble gas ions, and due to this, graphene becomes fundamentally transparent.

3.1.2 Crystal Growth

Growth of graphene in the form of a layer on a huge scale usually do not occur, but defect is essentially required, as in the case of chemical vapor deposition (CVD), defects take place naturally for growing the graphene layers. However, high-temperature growth makes possible by the relaxation and leads to thermal equilibrium so that defects can anneal in a rapid manner. Line defects are created when simultaneous nucleation of graphene layers occurs at different regions over a substrate.

3.1.3 Chemical Methods

When carbon atoms react with the non-carbon species in a graphene layer there are losses of atoms which result in defects. In this type of reactions oxidation is the most common one, and due to this, oxygen, hydroxyl, or carboxyl groups are attached to the graphene. In these chemical treatments highly defective surface-functionalized graphene is obtained by an oxygen group called graphene oxide [95] which are covered uniformly with hydroxyl or carboxylic groups. Moreover, at room temperature very few numbers of reactions are allowed because graphene is highly inert except for its boundaries.

3.2 Properties of Graphene with Defects

The chemical and electronic properties of graphene are immensely affected by defects. Moreover, from various simulations, it has been observed that the functional groups such as hydroxyl and carboxyl can have better attachment in the surface of graphene incorporated with vacancies defects [96]. Similarly, in the case of hydrogen saturated boundaries of graphene, the local reactivity is also enhanced substantially. The theoretical equations, i.e., Schrodinger equation in relation to electron will be replaced by Dirac equation for graphene induced with defects that directly influence the electronic structure. In almost all defective graphene scattering of the electron waves takes place and orientation of electron changes [96, 97].

4 Properties of Graphene-Based Polymer Composites

The researchers have focused on different kinds of polymeric composites comprising carbon-based nanomaterials, including CNTs, CF, graphene, graphene oxide, etc., and studied electrical and mechanical properties in the field of energy storage devices. In this section, we have discussed especially the properties of graphene as well as graphene-oxide-based composites using different polymer matrices. The graphene-based polymer composites might be useful for academic and industrial researchers for the development of various kinds of new graphene-filled polymer composite systems.

4.1 Poly(Vinyl Alcohol) (PVA)–Graphene Composites

Santos et al. [98] have reported polyvinyl alcohol-doped (PVA) ternary sulfonated graphene oxide (SGO) with graphite into polyethylene oxide (PEO) and poly(vinyl pyrrolidone) (PVP) via solution casting technique. It is observed that the swelling

ratio is decreased by 17 wt% of SGO composite membrane and lowers two orders of magnitude (0.18×10^{-6} cm^2 s^{-1}) of the permeability as compared to borohydride anion. These composite systems are characterized by scanning electron microscopy (SEM), transmission electron microscopy (TEM), X-ray diffraction (XRD), Fourier-transform infrared spectroscopy (FTIR), and Raman spectroscopy. The direct borohydride fuel cell (DBFC) is used due to its ease of processability, low energy consumption, simple to use and sustainable, as well as cost-effective, and also water is used as a solvent. It is also revealed that the interaction in acidic SGO and cross-linked polymer improved the membrane's mechanical resistance, ionic conductivity, and oxidative stability. In addition, the SGO-encapsulated PVA-PEO-PVP ternary membrane exhibits lower permeability of boro-hydride than that of the Nafion 117, which gives a higher selectivity. Cobos et al. [99] have successfully synthesized polyvinyl-alcohol (PVA)-silver (Ag)-graphene oxide (GO) (PVA-Ag NPs-GO) nanocomposite via a one-step process with L-ascorbic acid as a reducing agent with a mixture of $AgNO_3$, GO, and aqueous solution of PVA. It is observed that GO sheets grafted with spherical Ag NPs are uniformly dispersed in a polymer matrix. The glass transition temperature, crystallization temperature, mechanical, and water resistance properties of PVA composite are enhanced with the incorporation of Ag NPs-GO filler contents and also show antibacterial activity against *Escherichia coli* and *Staphylococcus aureus.* Similarly, they have also shown the homogeneous distribution of spherical silver nanoparticles over the surface of carbon substitute (10 nm in diameter) by an environmentally friendly process. Moreover, the thermogravimetric measurements signified the thermal stability of PVA composites as well as get enhanced by the incorporation of Ag NPs-GO. The Young's modulus and tensile strength of the composites significantly increased by incorporating filler particles, which is helpful for practical applicability in wound dressing [99–101]. Jain et al. [102] have reported on the effect of chemically reduced graphene oxide (RGO)-PVA matrix composite with various weight percentages of filler contents via a biomimetic approach. The microstructural analysis by scanning electron microscope (SEM) revealed better dispersion of RGO into the polymer matrix, and fibril alignment with high lamellar structure is observed. This incorporation of RGO to polymer matrix improved the tensile strength to 67.21 MPa as compared to that of pristine polyvinyl alcohol (PVA) matrix (33 MPa) (as shown in Fig. 4) [102, 103]. The degree of crystallinity and melting enthalpy of PVA-RGO composites are obtained from thermal analysis. It has been noticed that the incorporation of 1% RGO-PVA composites enhanced Young's modulus (5.53 GPA and 5.03 GPA) from the load penetration depth curve. The RGO shows load transfer to PVA matrix which enhances the modulus and tensile strength of RGO-PVA composite and decreased hardness which is found to be about 0.27 GPA. These RGO-PVA composite systems may be applied in the field of supercapacitance, bone regeneration, biosensors, etc. [103, 104].

Similarly, Khan et al. [105] have reported on sulfonated polyvinyl alcohol-aluminum oxide-graphene-platinum (SPVAAI-GR-PT) film by electroding with platinum using electro less plating technique. It has been observed that the ion exchange capacity (1.8 m eqg^{-1}) of the dry film and water uptake (125% at 45 °C for 10 h of drenching time) is superior as compared to other reported composites. The

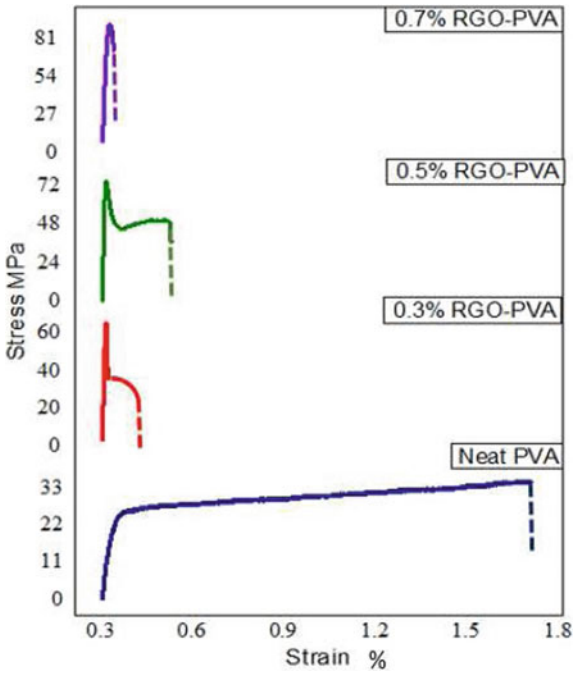

Fig. 4 Variation of stress vs. strain of RGO-incorporated PVA composite. Reprinted with permission from Ref. [102]

electro chemical, electromechanical, structural, morphological properties have been analyzed with various experimental techniques. However, it has good proton conductivity and high temperature stability with better electromechanical properties, which might be a better alternative for conventional polymer-based ionic polymer-metal composite (IPMC) actuator. In addition, the synthesized film has several potential applications in the domain of nano-electronics, actuators, sensors, supercapacitor, and robotics [106, 107].

4.2 Poly(Vinylidene Fluoride) (PVDF)–Graphene Composites

Kang et al. [108] have successfully fabricated MnO_2 doped graphene-based poly(vinylidene fluoride) (PVDF) composite systems for supercapacitor application by using a simple stirring and heating process. It is observed that 5 wt% of CBE shows higher specific capacitance (220 F g^{-1}) than that of the 5% PBE (202 F g^{-1}) at 0.5 Ag^{-1} with identical graphene contents, which is measured from galvanostatic charge–discharge plots (Fig. 5a, b). The cycling stability is found to be 90.07% (Fig. 5c) of the initial specific capacitance of 5% CBE, which is also retained after 1000 cycles. The chemical bond between graphene and PVDF improved electrochemical performance and lead to an effective electron pathway by bridging MnO_2

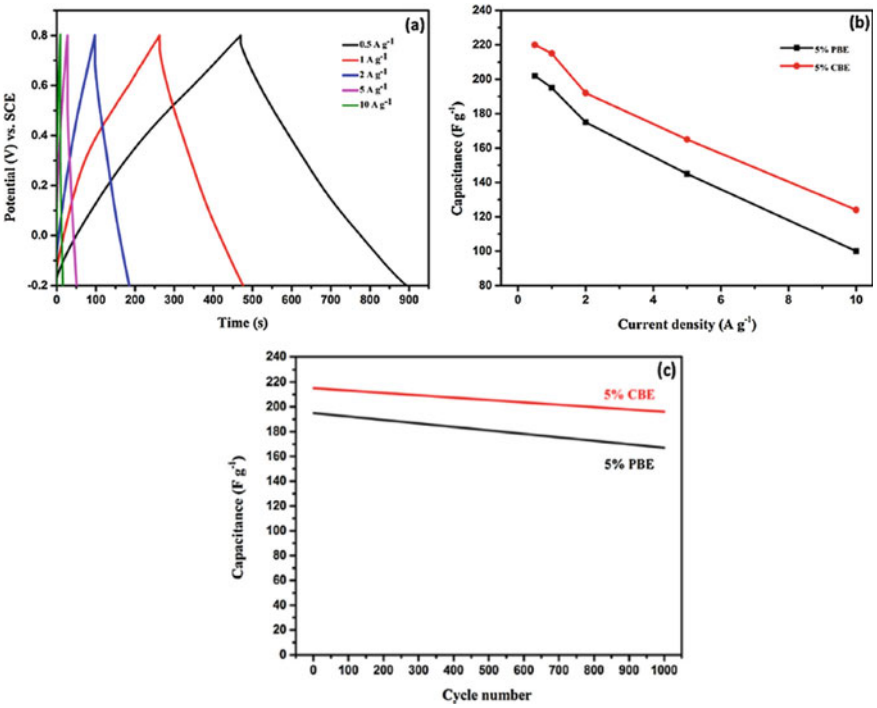

Fig. 5 Variation of **a** charge–discharge curves for 5% of CBE with various current densities, **b** rate capability of the 5% CBE and PBE, and **c** charge–discharge curve of the 5% CBE and PBE. Reprinted with permission from Ref. [108]

particles in the electrodes, which is responsible for the rapid electron transfer and low charge transfer resistance. The MnO_2 supercapacitor incorporated with a composite binder is subjected to cyclic voltammetry (CV) and galvanostatic charge–discharge process (Fig. 5), which shows an excellent electrochemical performance with a maximum specific capacitance of 220 F g^{-1} in 1 ^{mol} L^{-1} Na_2SO_4 electrolyte.

A ternary P(VDF-HFP)-polyaniline (PANI)-graphene oxide (GO) hybrid membrane (10 wt%, 25 wt%, and 40 wt%) was prepared by Hamid et al. [109] by using polymer electrolyte membrane (PEM) for lithium-ion battery. The scanning electron microscopy (SEM), X-ray diffraction (XRD), differential scanning calorimetry (DSC), and Fourier-transform infrared spectroscopy (FTIR) analyses have been performed and the electrochemical stability, porosity, and electrolyte uptake determined the effect of the incorporation of GO into P(VDF-HFP) polymer matrix. However, they revealed very high ionic conductivity ($10^4 \times 10^{-3}$ mS cm^{-1}) of P(VDF-HFP)-PANI membrane with tensile strength increased from 2.8 MPa to 8.8 MPa by the introduction of GO. The ternary P(VDF-HFP)-PANI-GO membrane shows porosity of 89.5% with excellent electrolyte uptake of 367.4%. Moreover, the ionic conductivity gets enhanced by the incorporation of polyaniline (PANI) and the

introduction of GO, which resulted in the improved thermal and mechanical properties of the membrane due to their π−π interaction and H-bonding. As an outcome, the electrochemical stability and cycling performance of P(VDF-HFP) membrane were enhanced. The (PVDF-HFP)-PANI-GO ternary polymer electrolyte membrane was found to be more stable even with decomposition voltage (5.6 V) and is nearly 100% Columbic efficiency after 10 cycles. The introduction of diglycidyl ether of bisphenol-A (DGEBA) functionalized reduced graphene oxide (rGO)-based epoxy composites with improved dielectric properties and thermal stability compared to neat graphene oxide (GO) and rGO sheet have been reported by Liao et al. [110]. It is observed that the dielectric constant of epoxy composite filled with 1 wt% of DGEBA-RGO sheets is 32 at room temperature at 1 kHz, which is nine times higher than that of neat epoxy (3.5). On the other hand, the dielectric loss of the resultant composites gets reduced (<1). This enhancement in dielectric properties is due to well-dispersed DGEBA-RGO and strong interaction between filler and polymer matrix, which may be attributed to an induced effective package of grafted DGEBA molecules on the graphene surface. In addition to this, the insulated DGEBA molecular layer affected the sheet contact directly resulting in the suppressed dielectric loss (<1). These high-performance composite films may be applicable in the field of embedded capacitors.

Mahaling et al. [111] have examined the dielectric properties of (Ag)-doped graphene oxide (GO)-poly(vinylidene fluoride-co-hexafluoropropylene) (PVDF-HFP) composites using solution casting technique. It is observed that the composite systems have a high dielectric constant (65) and diminished dielectric loss values (<1) at 10^2 Hz (Fig. 6a, b). However, the Ag nanoparticles as the conductive phase are persistently incorporated on the surface of graphene oxide (GO). The experimental results showed the formations of Ag layers on GO sheet with homogeneous distribution into the P(VDF-HFP) matrix were confirmed by field emission scanning electron microscopy (FESEM). Besides, the percolation threshold of 1.5 vol% of Ag-GO and Ag layer formed on the surface of GO sheet, which influenced with the enhancement of dielectric and electrical performance. These Ag encapsulated GO-P(VDF-HFP) composite systems may have useful application in the field of electronic capacitors.

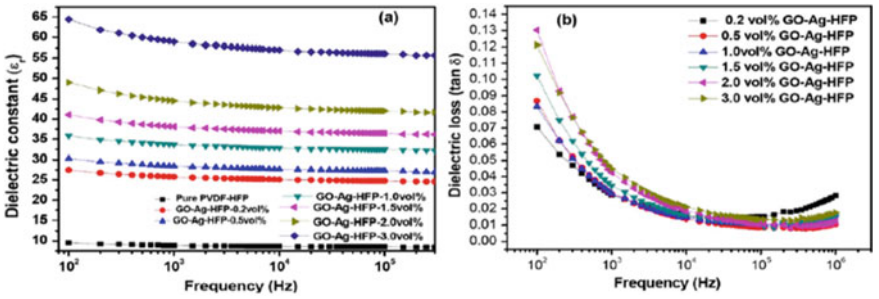

Fig. 6 Frequency dependence of **a** dielectric constant and **b** dielectric loss of Ag-GO-PVDF-HFP composites. Reprinted with permission from Ref. [111]

Chen et al. [112] have prepared a composite of reduced graphene oxide (rGO)-$CaCu_3Ti_4O_{12}$ (CCTO) in polyvinylidene fluoride (PVDF) by solution processing technique. It is observed that the composite has a high dielectric constant (40.4) and a low dielectric loss (0.08) at 1 kHz, when rGO and functionalized CCTO were 0.61 vol% and 12.5 vol%, respectively. In addition to this, the tunneling effects between rGO sheets play an important role in electrical conductivity and dielectric loss of the composite. This composite has application in designing and fabricating polymer composite for nonlinear dielectric and flexible electronic applications. He et al. [113] have developed poly(vinylidene fluoride) (PVDF)-polypyrrole (PPy)@graphene oxide (GO) composite via solution compounding processing. The resulting composite has higher electrical conductivity compared to two-phase PVDF-PPy composites. However, it is observed that the said composites have higher permittivity with a slight reduction in dielectric loss, which may have application in the field of energy storage. Li et al. [114] have fabricated polyvinylidene fluoride (PVDF) composite having high dielectric constant and low dielectric loss, which is obtained by incorporation of reduced graphene oxide(rGO) decorated with magnetic iron oxide (rGO@Fe_3O_4) on PVDF matrix by solution mixing and subsequent melt compression molding technique. This composite has been subjected to X-ray diffraction, Fourier-transform infrared (FTIR), thermogravimetric analysis (TGA), impedance analyzer, and magnetometer. They found that the dielectric constant becomes 1297 and the low dielectric loss is 0.26 at 100 $_{Hz}$ with 1.0 wt% RGO@Fe_3O_4 in the PVDF matrix. The excellent dielectric properties may be a consequence of core–shell structure and well dispersion of RGO@Fe_3O_4 in the PVDF matrix. These composites might be applicable in the field of mini capacitors. Fu et al. [115] have reported the development of polydopamine (PDA)-reduced graphene oxide (rGO) by self-polymerization and subsequent chemical reduction, then incorporated into PVDF matrix by solvent blending method. It has been seen that the dielectric constant of PVDF increases to 176 with 0.70 wt% rGO with a reduced tangent loss of 0.337, which is attributed to the reduction of concentration mobility of ionizable carboxyl group by PDA as depicted in Fig. 7a, b. These composites have good flexibility and

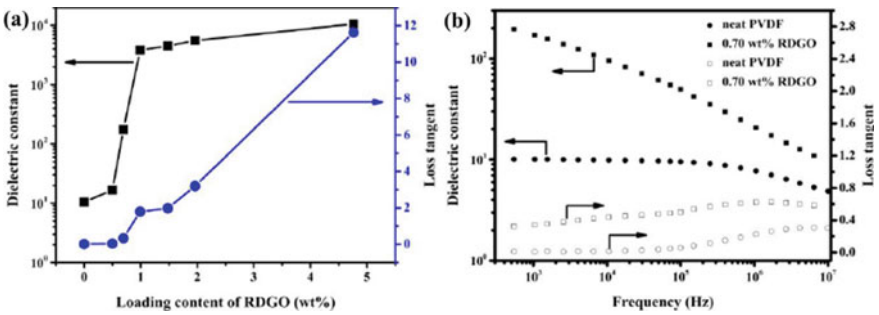

Fig. 7 Variation of **a** dielectric constant and **b** dielectric loss of polydopamine (PDA)-reduced graphene oxide (rGO) composites with 0.70 wt% of rGO contents. Reprinted with permission from Ref. [115]

better dielectric properties suitable for superior application in energy storage devices. The enhancement in dielectric constant is due to duplex interfacial polymerization of graphene–semiconductor interface and semiconductor–insulator interface [116].

Poly(vinylidene fluoride-co-hexafluoropropylene) (PVDF-HFP) incorporated with titanium dioxide-modified rGO (RGO-TiO_2-P(VDF-HFP) [PVDF-HFP] nanocomposite has been prepared by in situ assembling of TiO_2 on GO, which has been reported by Tong et al. [117]. It has been found that the increase in rGO-TiO_2 content increases the dielectric permittivity and low dielectric loss at low frequencies. Further, it is observed that the well-coated TiO_2 dielectric shell acted as an interparticle barrier to prevent direct contact with the graphene sheets. Tong et al. [118] have studied the preparation of poly(vinylidene fluoride-co-hexafluoropropylene) (PVDF-HFP) incorporated polyethylenimine (PEI) nanocomposite by solution casting method. The successful grafting of PEI on GO has been verified by infrared (IR), atomic force microscope (AFM), X-ray photoelectron spectroscopy (XPS), Raman spectroscopy, and thermogravimetric analysis (TGA). Moreover, the dielectric constant of the composite is found to be 67 (1000 Hz) with 8 wt% of rGO-PEI and low dielectric loss (0.12) at specific frequency regions. Li et al. [119] have reported the nanocomposite made from poly (vinylidene fluoride) (PVDF) and poly(vinyl pyrrolidone) (PVP)-anchored rGO (rGO@PVP) nanosheets via solution casting method. Further, the microstructure and dispersion in this nanocomposite have been investigated by atomic force microscope (AFM), X-ray photoelectron spectroscopy (XPS), thermogravimetric analysis (TGA), and Raman spectroscopy. However, the composite has a high dielectric permittivity of 622 and a dielectric loss of 0.2 near the percolation threshold at 100 Hz. This composite with improved dielectric properties and homogeneous dispersion leads to intercalation between rGO and PVDF matrix, and due to the presence of PVP, it resulted in the formation of micro and nano-capacitor structure. The PVDF has the growth of beta form crystal and when induced by the PVP space layer it suppresses the loss near the percolation threshold. These high dielectric constant and low dielectric loss composites may be integrated into electronic energy storage devices. Similarly, Wu et al. [120] have achieved a high dielectric constant of 364 and a low dielectric loss of 0.77 at 1 kHz by synthesizing chlorinated GO-PVDF composite. It is observed that the enhancement in dielectric and electrical conductivity is due to charge transfer complexes. The improved interfacial interaction between fillers and PVDF is due to hydrogen bonds and transformation of PVDF to beta-phase and dipolar interaction. It has been noticed that the tangent loss increases to 2.88 at 1 kHz with 0.4 vol% graphene. The dielectric properties of Cl-doped rGO-PVDF composites are due to the synergistic effect of several important modifications arising from the chlorination of GO sheets.

4.3 Epoxy-Graphene Composites

Prusty et al. [121] have reported on the improvement of flexural and interlaminar properties of carbon fiber-reinforced polymer (CFRP) composite by modification of

the surface of carbon fiber using graphene-oxide-based nanofiller (GBN) by electrophoretic deposition (EPD) technique. It has been seen that flexural and interlaminar strength of G-COOH-modified CFRP composite is 9.6% and 22.9% higher than that of control CFRP. The reinforcement mechanism involves esterification between G-COOH and epoxy, which enhanced filtration of epoxy as a result of improved interlocking between epoxy and carbon fibre. However, for a better understanding of the temperature-dependent mechanical behavior and various failure of micromechanism of the composite, they performed dynamic mechanical thermal analysis (DMTA) in the range of 30 °C–180 °C. The scanning electron microscopy (SEM) analysis indicated fiber pulled out to be the most prominent mode of failure in neat CFRP composite which is reduced in the case of G-COOH-modified CFRP composites. Simultaneously, the enhancement in flexural strength for polymer matrix beam reinforced with graphene and carbon filler at nano and micro level is taken place as compared to plain control beam reinforced with graphene. Wan et al. [122] have fabricated epoxy composite filled with graphene oxide (GO) diglycidyl ether of bisphenol-A functionalized GO (DGEBA-f-GO) sheet at various filler loading. It is identified that the presence of DGEBA improves the compatibility and dispersion of GO sheet in an epoxy matrix, while the strong interfacial interaction between sheets and epoxy matrix results in effective load transfer from the matrix to (DGEBA-f-GO). Meanwhile, it is observed that the tensile modulus and strength of epoxy composite with 0.25 wt% DGEBA-f-GO has increased from 0.15 ± 0.11 to 3.56 ± 0.08 GPa (13%) and 52.98 ± 5.82 to 92.94 ± 5.03 MPa (75%) respectively, compared to the neat epoxy resin and fracture toughness (29–41%). The neat GO and DGEBA-f-GO of 0.25 wt% loading produced 26% and 41% improvements in KIC values of epoxy composites, which indicate improved interfacial interaction between DGEBA-f-GO and matrix. The DMTA and TGA analyses indicate increased glass transition temperature and better thermal stability of DGEBA-f-GO-epoxy-based composites compared to two-phase GO-epoxy composite. Surnova et al. [123] have synthesized graphene oxide (GO)-based epoxy composite by homogeneous liquid phase transfer of GO into the epoxy resin resulting in uniform distribution of GO flakes within the epoxy matrix. The study of NPEL-128 epoxy resin curing by DDM showed that the introduction of GO into the epoxy resin exhibits an accelerating effect on the curing reaction. It is investigated that the storage modulus of epoxy matrix gets increased by 25.4% (3035 MPa) by the introduction of 0.2% GO as compared to neat epoxy polymer (2420 MPa). This enhancement is due to the highly exfoliated condition of GO in the matrix and covalent bonding between GO flakes and epoxy matrix at relatively low loading. Feng et al. [124] have synthesized reduced graphene oxide (RGO)@$Ni(OH)_2$, hexagonal boron nitride (h-BN) sheet (lateral size of 4.37 ± 1.68 μm and thickness of 80 ± 21 nm) hybrid in epoxy matrix composites using ultrasonication technique. These composites have high thermal conductivity (Fig. 8a) and flame retardancy properties, as confirmed by peak heat release rate, total heat release, and total smoke production (33.5%, 33.8%, and 43.0%) as compared to the neat epoxy. The RGO@$Ni(OH)_2$ hybrid in a matrix having good dispersion and interfacial interaction suppressed the stacking aggregation behavior of h-BN sheets with induced thermal conductivity (2.01 w/mK).

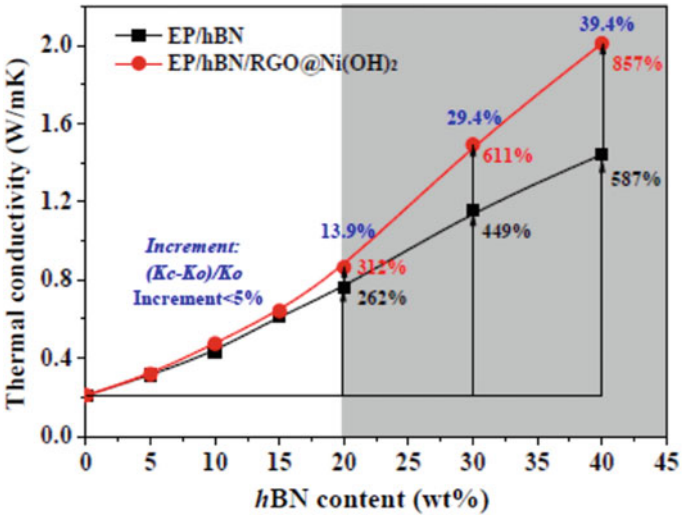

Fig. 8 **a** Thermal conductivity of EP-hBN and EP-hBN-RGO@Ni(OH)$_2$ composites as a function of h-BN contents. Reprinted with permission from Ref. [124]

Besides, improvement in the interfacial adhesive performance of dopamine-modified aramine fiber (AF) grafted with amino-functionalized graphene oxide using the secondary reaction of active hydrogen in polydopamine has been reported by Gong et al. [125]. It was found that this grafting is attributed to the increase in surface roughness and surface-active groups, polarity, and reactivity of polydopamine (PDA-AF surface), which is investigated by Fourier-transform infrared spectroscopy (FTIR), X-ray photoelectron spectroscopy (XPS), and scanning electron microscopy (SEM). The interfacial shear strength of AF-epoxy composite was enhanced by 34% after the incorporation of amino graphene oxide. This reinforcement of AF on GO may be a high-performance fiber, which can be used in electromagnetic interference shielding and environmental remediation.

4.4 Polystyrene (PS)–Graphene Composites

Zhang et al. [126] have developed polystyrene-grafted reduced graphene oxide (RGO-PS) composites via the emulsion polymerization process. It is observed that with an increase in the amount of grafted PS or RGO, the dielectric constant increases whereas dielectric loss remains constant. However, the composites containing RGOs with the highest amount of grafted PS show a low dielectric loss of 0.45 at 100 Hz and conductivity of 4.0410^{-9} S/cm, which is due to improved interfacial polarization induced by the PS layer. On the other hand, grafting of PS also increased the glass transition temperature of composite. Sun et al. [127] have prepared graphene

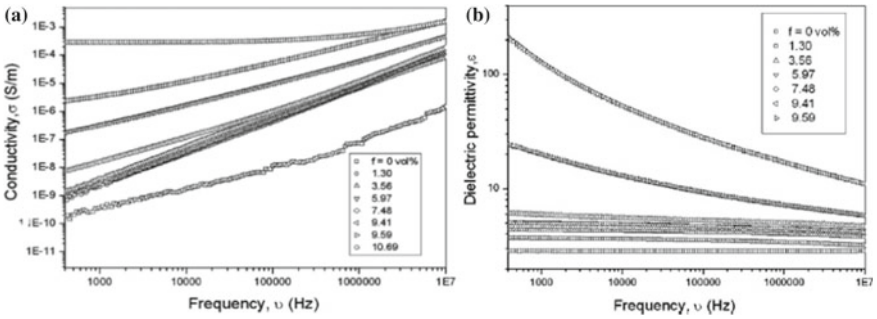

Fig. 9 Frequency dependence of **a** AC conductivity and **b** dielectric constant with different vol% of filler contents. Reprinted with permission from Ref. [128]

oxide (GO) and polystyrene (PS) nanocomposite via pickering emulsion polymerization technique characterized by transmission electron microscopy (TEM), scanning electron microscopy (SEM), and X-ray diffraction (XRD). It was noticed that GO-PS nanocomposite has higher crystallinity and better thermal stability than pure PS chain. These composites have several applications in electromechanical and coating industries. Graphene nanosheet Fe_3O_4(GNS-Fe_3O_4) hybrids have been successfully synthesized by He et al. [128] by one-step solvothermal reduction of iron(III) acetylacetonate [$Fe(acac)_3$] and GO simultaneously, then blended with syndiotactic PS (SPS) by solution blending method. It was investigated that the percolation threshold of GNS-Fe_3O_4 in SPS was 9.41 vol%. At the same time, the composite GNS-Fe_3O_4-SPS has a high dielectric permittivity of 123 at 10^3 Hz (Fig. 9b), which is nearly 42 times higher than pure SPS. Meanwhile, the AC electrical conductivity at 10^3 Hz increased from 3.6×10^{-10} S/m for pure SPS to 2.82×10^{-4} S/m for GNS-Fe_3O_4-SPS composite containing 10.69 vol% of GNS-Fe_3O_4 which showed that an insulator semiconductor transition (Fig. 9a). These composites have various applications in high-charge storage capacitor, electromagnetic interference shielding, and electromagnetic wave absorption.

Tu et al. [129] have developed graphene nanosheet (GN)–polystyrene (PS) latex nanocomposite system using the emulsification process, where the GO sheet is attached to PS particles through electrostatic adsorption. It was shown that the resultant composites have excellent electrical properties with a low percolation threshold as low as 0.054 vol% of GN sheet. Meanwhile, it was observed that the electrical conductivity was 46.32 S/m and thermal conductivity was 0.47 w/mk. This composite can be used in high-energy–density capacitors as dielectric film. Chen et al. [130] have synthesized polystyrene (PS)-Fe_3O_4@Thermally exfoliated and reduced graphene oxide (TGO) composite by solution blending method. The PS-Fe_3O_4-TGO composites are found to be of much higher electrical conductivity and electromagnetic interference (EMI) shielding effectiveness than PS-Fe_3O_4@RGO (reduced graphene oxide) composites due to better reduction of TGO than RGO. It was also revealed that the EMI shielding effectiveness of PS-Fe_3O_4-TGO composites is more than 30 Db in the frequency range of 9.8–12 $_{GHz}$ with 22.4% of graphene content.

This behavior is due to the combination of electrically conductive TGO sheets and magnetic Fe_3O_4 nanoparticles. Wang et al. [131] have prepared 2-poly(styrene-ran-butylene-b-styrene) (SEBS)-graphene oxide (GO) composites at different styrene segment content using the solution blending method. It is observed that with the addition of 0.5 wt% GO-enhanced tensile strength and modulus of SEBS-30 by 44% and 64%, SEBS-12 was increased by 24% and 39%. Moreover, the micro rack formation by GO increased the toughness and fibrillation of SEBS during the fracture process. Furthermore, the elongation at break and fracture toughness of SEBS-30 was increased by 10% and 64%, respectively.

Graphene oxide (GO)-reinforced polymer composite consisting of poly(4-styrene sulfonic acid) (PSSA) and polyvinyl alcohol (PVA) blend matrix has been synthesized by Deshmukh et al. [132] using the colloidal processing technique. These composites were successfully characterized by Fourier-transform infrared spectroscopy (FTIR), Raman spectroscopy, X-ray diffraction (XRD), UV–Visible spectroscopy, thermogravimetric analysis (TGA), polarized optical microscopy (POM), and scanning electron microscopy (SEM). It is observed that the resultant composites have a higher dielectric constant of 297.91 (50 Hz, 150 °C) with 3 wt% GO loading. Furthermore, the dielectric loss has increased to about 2.64 (50 Hz, 140 °C) with 3 wt% GO loading, which makes it efficient for energy storage application in electronic devices and embedded capacitors.

4.5 Polypropylene (PP)-Based Graphene Composites

Adloo et al. [133] have described the preparation of maleic anhydride grafted polypropylene (PP-MAH)-graphene-based composite via compression molding method, which was characterized by Fourier-transform infrared (FTIR), X-ray diffraction (XRD), atomic force microscopy (AFM) analysis. It is noted that the flexural strength and electrical conductivity is 44.28 MPa and 104.63 S/cm respectively, which is due to the formation of hydrogen bond between graphene and PP-MAH. Wang et al. [134] have reported about reduced graphene oxide-polypropylene (rGO-PP) composite by latex method, which has ultra-low percolation threshold at 0.033 vol% of filler content. However, the composite shows homogeneous dispersion of rGO nanosheet in PP matrix by analysis of scanning electron microscope (SEM). Moreover, there is a transition that occurs from insulator to conductor percolation with an increase in the rGO loading within the polymer matrix. Further, it was observed that the dielectric permittivity of the composite significantly increases as three orders of magnitude. The reduced graphene oxide-polypropylene (rGO-PP) composite with a high dielectric constant might be used as high-energy–density capacitors. Chen et al. [135] have fabricated multiwalled carbon-nanotubes-reinforced polypropylene conductive fibrous membrane via melt electrospinning technique. Initially, CNT is mixed with a small amount of paraffin liquid (PL) and then melt blended with PP matrix via melt electrospinning technique and

fibrous membrane with fiber diameter is about 1–3 μm. The microstructural analysis confirms the good orientation and well-dispersed CNTs in PP fiber by scanning and transmission electron microscopy after the addition of PL. These conductive fibrous membranes (CNT-PL-PP) have improved the tensile strength and modulus with superior electrical conductivity and better dielectric constant than that of the CNT-PP fibrous membrane with various percentages of CNT contents, as shown in Fig. 10a–c.

Ding et al. [136] have reported high, thermally conductive, three-dimensional polypropylene–graphene composites via in situ building technique. The composite shows higher thermal conductivity (10.93 Wm^{-1} K^{-1}). This is 55 times greater than that of the pristine PP matrix. Moreover, the polypropylene (PP)–graphene composites have excellent heat dissipation for LED and superior interaction between polypropylene and graphene through hydrogen bonding and π–π conjugate which reduced interfacial thermal resistance. The synthesized composite has wide applicability in the field of heat dissipation of high-power and highly integrated electronic devices. Guo et al. [137] have reported a low weight percentage of graphene nanoplatelets-reinforced polypropylene nanocomposites by using solution mixing

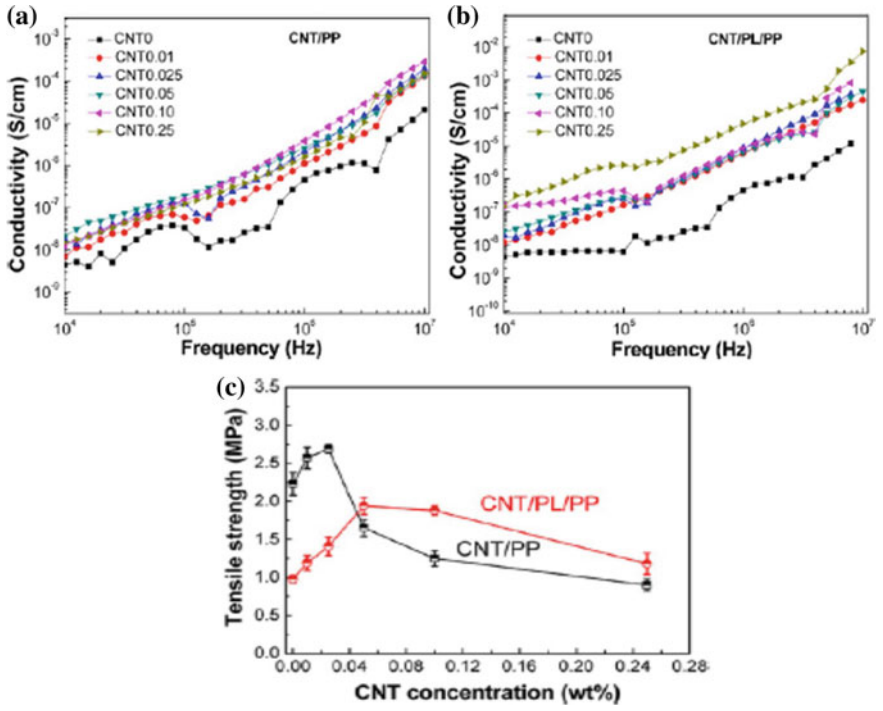

Fig. 10 Frequency dependence of **a**, **b** electrical conductivity and **c** tensile properties of the CNT-PL-PP electrospun fibrous membranes with various concentrations of CNT contents. Reprinted with permission from Ref. [135]

technique and it is widely used in the field of lightweight storage tanks. They studied the effect of physical, mechanical, and morphological performances of polypropylene with various weight percentages of graphene nanoplatelets into the polymer matrix with improved thermal stability and increased graphene contents. The storage modulus provides the elastic modulus of the nanocomposites, while the loss modulus is a measure of frictional losses, which is due to the motion of polymer chains [138]. Moreover, the magnitude of increase in storage modulus is lower than that of Young's modulus, which may be due to the difference in the measurement mode and resolution of instruments.

4.6 Polyimide (PI)-Based Graphene Composites

Chen et al. [139] have synthesized graphene oxide [GO-polyimide (PI)] composite by incorporation of GO into PI resin via in situ polymerization method. It has been observed that this composite has a high tensile strength of 40% for 0.5 wt% GO and tensile elongation of 32% which is three times greater than pure PI film. Further, it has an enhancement in thermal stability. This composite with improving dielectric, mechanical, and thermal properties has application in aerospace industries. Luong et al. [140] have studied the fabrication of polyimide (PI)-functionalized graphene (FGS) nanocomposite by in situ polymerization, which shows an improvement in mechanical and electrical conductivity. It has been observed that the PI/FGS composite has Young's modulus of 2.3 GPa, tensile strength of 131 MPa, and electrical conductivity in the order of 1.7×10^{-5} Sm^{-1}. Meanwhile, the composite can be used in microelectronics and aerospace industries. Kothurkar et al. [141] have fabricated graphene oxide-polyimide-based nanofiber composites via electrospinning technique. It is observed that the GO-PI nanofiber composites were characterized by Fourier-transform infrared spectroscopy, X-ray diffraction, Raman spectroscopy, thermogravimetric analysis, transmission electron microscopy (TEM), and high-resolution scanning electron microscopy (HRSEM). The results showed that GO is bunched up into a bead or spindle-like structure within the nanofiber. However, the dynamic mechanical analysis (DMTA) exhibited 2 wt% GO improved storage modulus (1.4×10^8 to 3.8×10^8 Pa) and also enhanced glass transition temperature (317–323 °C) than that of the pristine PI (as shown in Fig. 11). The thermogravimetric analysis (TGA) confirms superior thermal stability than that of a pristine polyimide matrix with increasing GO content. Ren et al. [142] have reported about high-performance polyimide nanofiber membrane by using electrospinning technique. The polyimide nanofibers have uniform dispersed and fiber diameters obtained in the range of 140–400 nm.

The PI nanofiber membranes exhibited better thermal stability with initial decomposition temperature (T_d) (544.4 °C) and heat resistance temperature (T_{HRI}) (198.8 °C). The mechanical performance of the nanofiber membranes is found with reasonable tensile strength (10.5 MPa) and Young's modulus (927.6 MPa). Further,

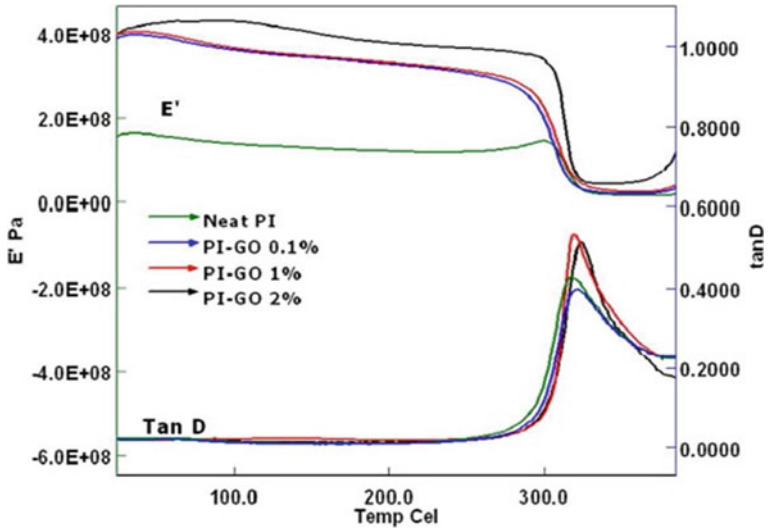

Fig. 11 Dynamic mechanical analysis of PI-GO composite with various weight percentage (0% (neat PI), 0.1%, 1.0%, and 2.0%) of GO contents. Reprinted with permission from Ref. [141]

the filtration performance of the nanofiber membranes showed the best filtration efficiency of 90.4%. These electrospun PI nanofiber membranes could be a promising candidate for hot gas filtration.

4.7 Polyurethane (PU)-Based Graphene Composites

Pokhreal et al. [143] have studied the mechanical properties of graphene nanoplatelets (GNPs), graphene oxide, and functionalized graphene sheets (FGS) incorporated into PU by in situ polymerization. It has been found that due to strong interaction of FGS with PU and 2 wt% of GO-PU the composite has high modulus (25.8 MPa) than GMPs with PU. It has been observed that the FGS/PU composite has high Young's modulus (213%) and high tensile strength (17%) than neat PU (Fig. 12). This enhancement is due to the increased number of hydroxyl groups on the surface of FGS than GO produced with a heavily PU-coated graphene sheet, which resulted in an interface for the stress transfer from PU to FGS. Lu et al. [144] have reported the synthesis of graphene(G)–polymer(P) composite to assess the force separation response of interface between the graphene and polymer matrix with polymers like polyethylene (PE), polyurethane (PU), and polystyrene (PS) by simulation process. However, for comparison a theoretical model proposed by Jiang et al. [145] was suggested, i.e., the interference based on cohesive law model. Meanwhile, it was found that the G/PU system has a weak interface as compared to G/PE and G/PS which helps in determining the mechanical properties, but the interfacial strength of each G/P matrix

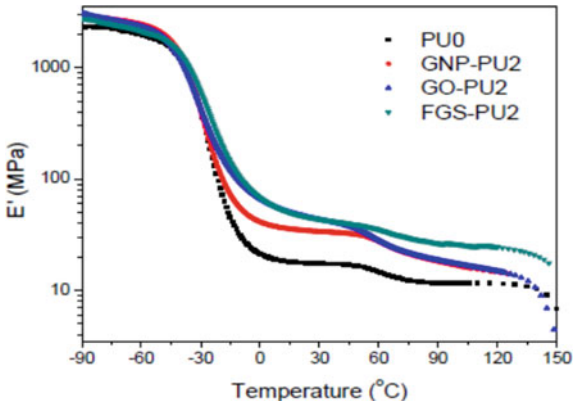

Fig. 12 Dynamic storage modulus with temperature for neat PU and 2 wt% of GO, FGS-based PU composites. Reprinted with permission from Ref. [143]

is greater than pure polymer. Sadasivuni et al. [146] have reported the formation of nanocomposite of polyurethane (PU) with hydrophilic graphene oxide (GO) and hydrophobic-modified GO (m-GO) by the solution mixing method. It has been seen that there is an increase in the dielectric permittivity of PU-mGO nanocomposite as compared to PU/GO, which confirmed more effective dispersion of thin exfoliated sheet of mGO in PU, characterized by scanning electron microscope (SEM) and X-ray diffraction (XRD). Meanwhile, the viscoelastic behaviors are studied by Kraus and Maier and Goritz models. These nanocomposites have application in capacitors. It is found that the stiffness and toughness are increased without any deterioration in the storage modulus.

5 Conducting Polymer-Based Graphene Composites

Conducting-polymer-filled graphene composites have much significant attention in both academic and industrial fields owing to their elevated conductivity, ease of processing, and multifunctional properties. There are several conducting polymer families such as PANI, polypyrrole, and polythiophene generally used as matrices. In this section, the main focus is on conducting polymer-based graphene composites and the subsections are devoted to summarizing their properties and applications in the field of energy storage devices.

5.1 Polyaniline (PANI)-Based Graphene Composites

Gupta et al. [147] have synthesized hybrid film of electrochemically processed graphene nanosheets with electrochemically synthesized (ErGO) conducting polymers polypropylene (ppy) and polyaniline (PANI) by layer-by-layer approach (LBL).

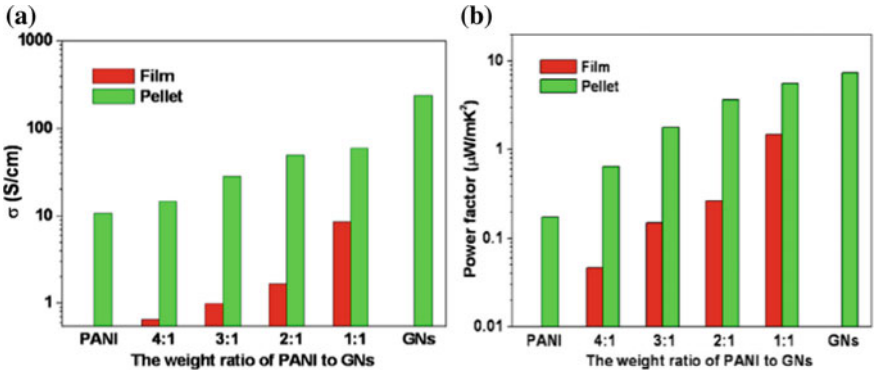

Fig. 13 Variation of **a** electrical conductivity and **c** power factor for PANI-GNs composite with various GNs contents. Reprinted with permission from Ref. [148]

It has been found that there is an increase in the mechanical properties of polymers due to the synergistic effect promoted by nanostructure morphology. The surface topology, chain ordering, residual stress distribution, force curve, and force volume imaging can be done by micro Raman spectroscopy, Raman mapping, atomic force microscopy (AFM), and force spectroscopy. Further, the force curve shows the enhancement in the spring constant (K) for the hybrids. Meanwhile, it was found that the mechanical properties get increased in the given order PANI/ErGO > PPy/ErGO > PANI/GO > PPy/GO > PANI > PPy. However, these hybrids are used in electrolyte-free or dry high energy storage density for dielectric capacitors and might be used in photovoltaic and aerospace device applications. Du et al. [148] have synthesized polyaniline (PANI)-graphene nanosheet (GNS) thermoelectric bulk composite pellets and film in the weight ratio ranging from 4:1 to 1:1, which gives rise to an increase in the power factor (Fig. 13c). It has been investigated that the electrical conductivity of both pellets and films are enhanced from 14.76 to 5889 S/cm and 0.66 to 8.63 S/cm, respectively, which may be due to the larger electrical conductivity of GNs pellet (as shown in Fig. 13a). As a result, this power factor of the pellets and films increased from 0.64 to 5.60 and 0.005 to 1.47 $\mu Wm^{-1} k^{-2}$. Further, the increase in carrier mobility leads to conducting polymer-inorganic composites, which have more usefulness in the field of thermoelectric application.

Haldar et al. [149] have reported the introduction of graphene into the stable matrix of MnO_3O_4-polyaniline composite, which has the applicability in supercapacitors with electrodes having a specific capacitance of 1000 Fg^{-1}. Meanwhile, the composite has good cycling stability of 97%. The initial capacitor at a current density of 25 Ag^{-1} for 3000 cycles is due to the connected percolated conductive path originating from dispersed graphene sheets. It has been found that the energy density and power density were 24.9 Wkg^{-1} and 900 Wkg^{-1}, respectively, at a current density of 1 Ag^{-1}. Gomez et al. [150] have fabricated graphene (G)-polyaniline (PANI) nanocomposite film via wet polymerization method for chemical application, which is characterized by Raman, scanning electron microscopy (SEM), high-resolution

transmission electron microscopy (TEM), FTIR, and cyclic voltammetry (CV) at different ratios of graphene and aniline monomer. It has been found that the specific capacitance of G-PANI nanocomposite is 300–500 Fg^{-1} at a current density of 0.1 Ag^{-1}. These composites have application in supercapacitors and packaging to qualification for portable system application. Further, graphene-PANI in the 1:2 ratio gives good cyclic stability. Wang et al. [151] have synthesized a high-performance electrode material of fibrillar PANI doped with graphene oxide (GO) via in situ polymerization method. It has been investigated that the nanocomposites have a high conductivity of 10 Scm^{-1} at 295 K for a mass ratio of aniline/GO (100:1). Furthermore, the specific capacitance is high at 531 F/g in a potential range from 0 to 0.45 V.

The structure and morphology have been investigated by energy-dispersive X-ray technique (EDX), scanning electron microscopy (SEM), and transmission electron microscopy (TEM). This composite can be used as supercapacitor and in other power source system. Jin et al. [152] have designed sulfonated graphene polyaniline nanofiber (SGEPA) composite via oil/water interfacial polymerization whose chemical structure is characterized by scanning electron microscopy (SEM) and high-resolution transmission electron microscopy (TEM). More importantly, the composite shows a better electrochemical performance than pure aniline nanofibers. It has been found that there is a high specific capacitance of 962 f/g at a potential scanning rate of 2 mv/s and high cycle stability of about 78% after 100 cycles. Meanwhile, it also exhibits a high energy density of 68.86 wh/kg at a power density of 102 w/kg. These properties help this composite in the application of supercapacitors. Ansari and co-workers have been successfully reported that highly conductive graphene/polyaniline nanocomposites can be prepared by the in situ oxidative polymerization of aniline in the presence of cetyltrimethylammonium bromide [153]. Because of $\pi-\pi$ interactions between PANI and GN, the distribution of GN is uniform in the matrix of PANI and obtained high electrical conductivity. Due to the conducting nature of GN and PANI, high electrical conductivity may be observed. Moreover, they have noticed that at room temperature, pTSA-doped GN-PANI composites exhibited enhanced electrical conductivity, i.e., 26.5 S/cm than PANI doped with inorganic acids [154]. Due to the additive/synergistic effect of GN and PANI, they show high electrical conductivity.

5.2 *Polypyrrole (PPy) and Polythiophene (PTh)-Based Graphene Composites*

Wang et al. [155] have investigated the polypyrrole (PPy) layers of intercalated graphene sheets by in situ intercalative chemical polymerization with different graphene and polypyrrole ratios, characterized by Fourier-transform infrared spectroscopy (FTIR), X-ray diffraction (XRD), Raman spectroscopy, and transmission electron microscope (TEM). It has been observed that the prepared graphene–PPy

composite with mass ratio 1:10 displayed the best electrochemical properties which have high specific capacitance and good cycling stability during charge–discharge processes which are used as supercapacitor electrode due to the homogeneous intercalation of PPy layers on graphene substrate. Further, these supercapacitors have a specific capacitance of 650 fg^{-1} at current density of 0.45 Ag^{-1}, high energy density of 54.0 $whkg^{-1}$ at 1 ^{mA} current, and the highest power density of 778.1 wkg^{-1} at 5 mA current, and the cycling stability is 95% specific capacitance retained after 5000 cycles. Liu et al. [156] have reported the conductivity of polypyrrole fiber-graphene composites to be increased (141 S/cm), which is much better than the pure pyrrole fiber. Ding et al. have successfully reported that graphene/polypyrrole composite fiber is selected as an ideal choice for the fiber-based electrochemical supercapacitor due to its conductivity which is about 137–144 S/m, measured by probe method [157]. Li et al. [158] have fabricated poly [3-(2-(2-(2-(2-(diethanolamino)ethoxy)ethoxy) ethoxy ethoxy) thiophene] (PD4ET)-g-GO nanocomposite by esterification reaction, which is characterized by Fourier-transform infrared (FTIR), X-ray diffraction (XRD), Raman, and X-ray photoelectron spectroscopy (XPS). It has been seen that the specific capacitance of the composite is 971 f/g at a current density of 1 A/g. Meanwhile, the cycling stability shows that the PD4ET-g-GO-based capacitor retained 98% of its initial capacitance within 1000 consecutive charge–discharge cycles, which indicate a good cycling stability. Further, the composites have excellent electrochemical performance, which can be used as a power supplier in red LED diode in series connection. Nayebi et al. [159] have studied the mechanical properties of graphene-polythiophene nanocomposite by molecular dynamic simulation by relax force field. It has been investigated that the mechanical characteristics of tension along the zigzag orientation are higher than any other direction. Furthermore, by increasing the weight concentration of graphene in composite, Young's modulus and breaking stress get enhanced. However, Young's modulus decreases with an increase in temperature and defect in graphene structure. Further, with defect concentration, elastic modulus decreases gradually. Poly (3-hexylthiophene) P3HT with low molecular weight (Mn 6000)/graphene composite has been fabricated by Laguchi et al. [160] using in situ polymerization. It has been investigated by FTIR, atomic force microscopy (AFM), and field-emission scanning electron microscope (FE-SEM) that the P3HT/graphene complex has flat and ultrathin multilayered graphene of approximately <10 nm in thickness. However, the composite has high electrical conductivity. Alabadi et al. [161] have prepared GO-(thiophene-2,5-diyl-co(benzylidene)(TB) composite by in situ polymerization. It has been observed that the composite has good capacitive performance in alkali aqueous electrolytes, less internal resistance, and high specific capacitance (296 fg^{-1}) at a current density of 0.3 Ag^{-1}. Furthermore, over 91.86% of the long-term stability is retained after repeating the galvanostatic charge/discharge over 4000 cycles, which indicates high cycle stability. More importantly, a large energy density of up to 148 $Whkg^{-1}$ at a power density of 41.6 Wkg^{-1} of the GO-TB-based three-electrode device is obtained with alkali aqueous electrolytes.

6 Summary

The graphene-based polymeric composites have become potential candidates for application in various technological fields due to their outstanding physical and chemical properties. Graphene is the most significant among members of carbon family having sp^2 hybridized two-dimensional carbon-based nanofillers with the honeycomb crystal lattice. These composites have significantly improved mechanical, thermal, and electrical performances with apposite applicability in electronic, electromagnetic interference shielding devices, tissue engineering, sensor, power storage, supercapacitors, etc. However, the graphene-based polymer composites have better dispersion and homogeneity due to superior chemical interaction between the particles and polymer matrix, which resulted in improvement in the overall performances of the composite systems. In this chapter, emphasis is especially on the electrospinning processing technique of graphene and the attractive properties of various polymer-based graphene composites. These graphene-based materials have opened a new dimension for the production of low-cost, lightweight, easy processing, and high-performance composites with a wide range of applications for industrial and academic researchers.

References

1. Costa, P. et al. High-performance graphene-based carbon nanofiller/polymer composites for piezoresistive sensor applications. Compos. Sci. Technol. **153**, 241-252 (2017).
2. Sankaran, S., Deshmukh, K., Ahamed, M. B. & Pasha, S. K. K.Recent advances in electromagnetic interference shielding properties of metal and carbon filler reinforced flexible polymer composites: A review.Compos. Part A: Appl. Sci. Manuf. **14**, 49-71 (2018).
3. Lightcap, I.V. & Kamat, P. V.Graphitic design: prospects of graphene-based nanocomposites for solar energy conversion, storage, and sensing. Acc. Chem. Res. **46**, 2235-2243 (2013).
4. Lei, Z., Christov, N. & Zhao, X. S. Intercalation of mesoporous carbon spheres between reduced graphene oxide sheets for preparing high-rate supercapacitor electrodes. Energy Environ. Sci.**4**, 1866-1873 (2011).
5. Evanoff Jr, D. D. & Chumanov, G.Synthesis and optical properties of silver nanoparticles and arrays. Chem. Phys. Chem., **6**, 1221-1231 (2005).
6. Winey, K.I. & Vaia, V.Polymer nanocomposites. MRS Bull.**32**, 314-322 (2007).
7. Yin, Z. et al. Graphene-Based Materials: Synthesis, Characterization, Properties, and Applications.Nano-Micro Small **7**, 1876-1902 (2011).
8. Tong, X., Li, N., Zeng, M. & Wang, Q. Organic phase change materials confined in carbon-based materials for thermal properties enhancement: Recent advancement and challenges. Renew. Sust. Energ. Rev.**108**, 398-422 (2019).
9. Huang, Y., Liang, J. & Chen, Y. An overview of the applications of graphene-based materials in supercapacitors. Small, **8**, 1805-1834 (2012).
10. Khan, M. et al. Graphene based metal and metal oxide nanocomposites: synthesis, properties and their applications.J. Mater. Chem. A **3**, 18753–18808 (2015).
11. Stankovich, S. et al. Graphene-based composite materials. Nature **442**, 282-286 (2006).
12. Xiao, X. C., Xie, T. & Cheng, Y.T. Self-healable graphene polymer composites. J. Mater. Chem. **20**, 3508-3514 (2010).

13. Chen, S., Skordos, A. & Thakur, V. K. Functional nanocomposites for energy storage: Chemistry and new horizons. Mater. Today Chem. **17**, 100304(2020).
14. Sengupta, R., Bhattacharya, M., Bandyopadhyay, S. & Bhowmick, A. K.A review on the mechanical and electrical properties of graphite and modified graphite reinforced polymer composites. Prog. Polym. Sci. **36**, 638–670 (2011).
15. Liang, C. et al. Constructing interconnected spherical hollow conductive networks in silver platelets/reduced graphene oxide foam/epoxy nanocomposites for superior electromagnetic interference shielding effectiveness. Nanoscale **11**, 22590-22598 (2019).
16. Lee, C., Wei, X., Kysar, J. W. & Hone, J. Measurement of the elastic properties and intrinsic strength of monolayer graphene. Science **321**, 385-388 (2008).
17. Kuilla,T. et al. Recent advances in graphene based polymer composites. Prog. Polym. Sci. **35,** 1350–1375(2010).
18. Cui, Y., Kundalwal, S. I. & Kumar, S. Gas barrier performance of graphene/polymer nanocomposites. Carbon **98**, 313-333 (2016).
19. Novoselov, K.S. et al. Electric field effect in atomically thin carbon films. Science **306**, 666-669 (2004).
20. Pang, S., Hernandez, Y., Feng, X. & Mullen, K. Graphene as transparent electrode material for organic electronics. Adv. Mater. **23**, 2779-2795 (2011).
21. Iwan,A. & Chuchmała, A. Perspectives of applied graphene: Polymer solar cells. Prog. Polym. Sci. **37**, 1805-1828 (2012).
22. Usuki, A. et al. Composite material containing a layered silicate. US Pat. 889885 (1989).
23. Garcia, N. J. & Bazan, J. C. Electrical conductivity of montmorillonite as a function of relative humidity: La-montmorillonite. Clay Miner. **44**, 81-88 (2009).
24. Bao, Y.Z.,Cong, L.F.,Huang, Z.M. & Weng, Z.X. Preparation and proton conductivity of poly (vinylidene fluoride)/layered double hydroxide nanocomposite gel electrolytes. J. Mater. Sci. **43**, 390-394 (2008).
25. Ivanov, R. et al. PLA/Graphene/MWCNT composites with improved electrical and thermal properties suitable for FDM 3D printing applications. Appl. Sci. **9**, 1209 (2019).
26. Paszkiewicz, S. et al. A. Enhanced Functional Properties of Low-Density Polyethylene Nanocomposites Containing Hybrid Fillers of Multi-Walled Carbon Nanotubes and Nano Carbon Black. Polym. **12**, 1356 (2020).
27. Achaby, M. El. & Qaiss, A. Processing and properties of polyethylene reinforced by graphene nanosheets and carbon nanotubes. Mater. Design. **44**, 81–89 (2013).
28. Neubauer, E., Kitzmantel, M., Hulman, M. & Angerer, P. Potential and challenges of metal-matrix-composites reinforced with carbon nanofibers and carbon nanotubes. Compos. Sci. Technol. **70**, 2228-2236 (2010).
29. Kim, J. H. et al.Simple and cost-effective method of highly conductive and elastic carbon nanotube/polydimethylsiloxane composite for wearable electronics. Sci. Rep. **8**, 1375 (2018).
30. Wang, Y. et al. Effect of nano-scale Cu particles on the electrical property of CNT/polymer nanocomposites. Compos. Part A: Appl. Sci. Manuf.**143**, 106325 (2021).
31. Balkanloo, P. G., Mahmoudian, M.&Hosseinzadeh, M. T. A comparative study between MMT-Fe_3O_4/PES, MMT-HBE/PES, and MMT-acid activated/PES mixed matrix membranes. Chem. Eng. J.**396**, 125188 (2020).
32. Araby, S. et al. Recent advances in carbon-based nanomaterials for flame retardant polymers and composites. Compos. Part B: Eng.**212**, 108675(2021).
33. Thakur, K. &Kandasubramanian, B. Graphene and graphene oxide-based composites for removal of organic pollutants: A review. J. Chem. Eng. Dat. **64**, 833-867 (2019).
34. Guo, Y., Bao, C., Song, L., Yuan, B. & Hu,Y. In Situ Polymerization of Graphene, Graphite Oxide, and Functionalized Graphite Oxide into Epoxy Resin and Comparison Study of On-the-Flame BehaviorInd. Eng. Chem. Res. **50**, 7772-7783 (2011).
35. Dai, J., Wang, G., Ma, L. & Wu, C. Study on the surface energies and dispersibility of graphene oxide and its derivatives. J. Mater Sci. **50**, 38953907 (2015).
36. Cui, J., Xiong, Z., Qiu, H., LI, J. & Yang, J. Functionalized graphene oxide: Carrier for corrosion inhibitor and barrier in waterborne epoxy coatings. Compos. Part A: Appl. Sci. Manuf. **144**, 106354 (2021).

37. Zong, P. et al. Effect of aminopropylisobutyl polyhedral oligomeric silsesquioxane functionalized graphene on the thermal conductivity and electrical insulation properties of epoxy composites. RSC Adv. **6**, 10498-10506 (2016).
38. Persano, L., Camposeo, A.,Tekmen, C. & Pisignano, D. Industrial upscaling of electrospinning and applications of polymer nanofibers: A review. Macromol. Mater. Eng. **298**, 504-520 (2013).
39. He, X. X. et al. Near-field electrospinning: progress and applications. Phys. Chem. C **121**, 8663-8678 (2017).
40. Zhang, L. F., Aboagye, A. & Kelkar, A. A review: carbon nanofibers from electrospun polyacrylonitrile and their applications. J. Mater. Sci. **49**, 463-480 (2014).
41. Wang, X., Yu, J., Sun, G. & Ding, B. Electrospun nanofibrous materials: a versatile medium for effective oil/water separation. Mater. Today **19**, 403-414 (2015).
42. Kim, J. F.,Kim, J. H.,Lee, Y. M. & Drioli, E. Thermally induced phase separation and electrospinning methods for emerging membrane applications: A review. Alche J. **62**, 461-490 (2016).
43. Mirjalili M. & Zohoori, S. Review for application of electrospinning and electrospun nanofibers technology in textile industry. J. Nanostructures Chem. **6**, 207-213 (2016).
44. Zhang, C. L. & Yu, S. H. Nanoparticles meet electrospinning: recent advances and future prospects. Chem. Soc. Rev. **43**, 4423-4448 (2014).
45. Bhardwaj, N. S. C. Kundu, Electrospinning: a fascinating fiber fabrication technique. Biotechnol. Adv. **28**, 325 (2010).
46. Chen, Z., Xin, B.,Wu, X.,Wang, X. &Du, W. Preparation and characterisation of PSA/CNT composites and fibres. Fibres Text. East. Eur. **94**, 21-25 (2012).
47. Yu, J., Xin, B. & Shen, C. Preparation and characterization of PSA/PEDOT conductive composite yarns. Text. Res. J., **87** (5), 528-541 (2017).
48. Chen, W. J., Xin, B. J. & Wu, X. J. Fabrication and characterization of PSA nanofibers via electrospinning. J. Ind. Text. **44**, 159-179 (2014).
49. Garg, K. & Bowlin, G. L. Electrospinning jets and nanofibrous structures.Biomicrofluidics**5**, 013403 (2011).
50. I. F. Wahab et al. Electrospun graphene oxide-based nanofibers. Adv. Carbon Nanostructures, 101–120 (2016).
51. Bao, Q. et al. Atomic-layer graphene as a saturable absorber for ultrafast pulsed lasers. Adv. Funct. Mater. **19**, 3077-3083 (2009).
52. Das, S. et al .Electrospinning of polymer nanofibers loaded with noncovalently functionalized graphene. J. Appl. Polym. Sci. **128**, 4040-4046 (2013).
53. Kim, S. Y., Kim, B. H.,Yang, K. S.& Kim, K. Y. The formation of silica nanoparticles on the polyacrylonitrile-based carbon nanofibers by graphene via electrospinning. Mater. Lett. **71**, 74-77 (2012).
54. Correa, E., Moncada, M .E.,Gutiérrez,O. D.,Vargas, C. A. & Zapata, V. H. Characterization of polycaprolactone/rGO nanocomposite scaffolds obtained by electrospinning. Mater. Sci. Eng. C Mater. Biol. Appl. **103**, 109773(2019).
55. Guo, Y. et al. Significantly enhanced and precisely modeled thermal conductivity in polyimide nanocomposites with chemically modified graphene via in situ polymerization and electrospinning-hot press technology. J. Mater. Chem. C **6**, 3004-3015 (2018).
56. Hou, W. et al. Preparation and physico-mechanical properties of amine-functionalized graphene/polyamide 6 nanocomposite fiber as a high performance material. RSC Adv. **4**, 4848-4855 (2014).
57. Ehteshami, S., Feizbakhsh, A., Sarrafi, A. H. M., Panahi, H. A. & Roostaie, A. An electrospun polyamide/graphene oxide nanocomposite as a novel fiber coating. Anal. Methods **10**, 2123-2128 (2018).
58. Karumuthil, S. C., Rajeev, S. P., Valiyaneerilakkal, U., Athiyanathil, S. & Varghese, S. Electrospun Poly(vinylidene fluoride-trifluoroethylene)-Based Polymer Nanocomposite Fibers for Piezoelectric Nanogenerators. ACS Appl. Mater. Interfaces **11**, 40180-40188 (2019).

59. Nieto, A., Dua, R., Zhang, C., Boesl, B.& Ramaswamy, S.Three dimensional graphene foam/polymer hybrid as a high strength biocompatible scaffold. Adv. Functional Mater. **25**, 3916-3924 (2015).
60. Samad, Y. A. Li, Y. Alhassan, S. M. & Liao, K. Novel graphene foam composite with adjustable sensitivity for sensor applications.ACS Appl. Mater. Interf. **7,** 9196–9202 (2015).
61. Sun, H. B., Yang, J., Zhou, Y. Z., Zhao, N. & Li, D. Preparation of reduced graphene oxide films by dip coating technique and their electrical conductivity. Mater. Technol. **29,** 14-20 (2014).
62. Fang, M. et al. Preparation of highly conductive graphene-coated glass fibers by sol-gel and dip-coating method. J. Mater. Sci. Technol., **3**, 1989-1995 (2019).
63. Chatterjee, A., Kumar, M. N. & Maity, S. Influence of graphene oxide concentration and dipping cycles on electrical conductivity of coated cotton textiles. J. Text. Inst. **108**, 1910-1916 (2017).
64. Berendjchi, A., Khajavi, R., Yousefi, A. A. & Yazdanshenas, M. E. Surface characteristics of coated polyester fabric with reduced graphene oxide and polypyrrole. Appl. Surf. Sci. **367**, 36-42 (2016).
65. Liu, X. et al. Fabricating conductive poly(ethylene terephthalate) nonwoven fabrics using an aqueous dispersion of reduced graphene oxide as a sheet dyestuff. RSC Adv. **4**, 23869-23875 (2014).
66. Kongahge, D., Foroughi, J., Gambhir, S., Spinks, G. M. & Wallace, G. G. Fabrication of a graphene coated nonwoven textile for industrial applications. RSC Adv. **6**, 73203-73209 (2016).
67. B. Thomas, H. J. Maria, G. George, S. Thomas, N.V. Unnikrishnan, K. Joseph, A novel green approach for the preparation of high performance nitrile butadiene rubber-pristine graphene nanocomposites. Compos. Part B Eng. **175**, 107174 (2019).
68. Bahrami, S., Solouk, A., Mirzadeh, H. & Seifalian, A. M. Electroconductive polyurethane/graphene nanocomposite forbiomedicalapplication. Compos. Part B Eng. **168**, 421-431 (2019).
69. Fan, J. et al. Gum arabic assisted exfoliation and fabrication of Ag–graphene-based hybrids. J. Mater. Chem. **22**, 13764-13772 (2012).
70. Johnson, D. W., Dobson, B. P.& Coleman, K. S. A manufacturing perspective on graphene dispersions. Curr. Opin. Colloid Interface Sci. **20**, 367-382 (2015).
71. Konios, D., Stylianakis, M. M., Stratakis, E. & Kymakis, E. Dispersion behaviour of graphene oxide and reduced graphene oxide. J. Colloid Interface Sci. **430**, 108-112 (2014).
72. Yang, X. et al. A high-performance graphene oxide-doped ion gel as gel polymer electrolyte for all-solid-state supercapacitor applications. Adv. Func. Mater. **23**, 3353 (2013)
73. Fattah, N. et al. An approach to solid-state electrical double layer capacitors fabricated with graphene oxide-doped, ionic liquid-based solid copolymer electrolytes. Mater. **9**, 450 (2016).
74. Mohammed, H. A. et al. Fabrication and characterizations of a novel etched-tapered single mode optical fiber ammonia sensors integrating PANI/GNF nanocomposite.Sens. Actuators B: Chem. **287**, 71-77 (2019).
75. Soltani-kordshuli, F., Zabihi, F. & Eslamian, M. Graphene-doped PEDOT: PSS nanocomposite thin films fabricated by conventional and substrate vibration-assisted spray coating (SVASC). Eng. Sci. Technol. Int. J. **19**, 1216-1223 (2016).
76. Jaworek, A. Electrospray droplet sources for thin film deposition. J. Mater. Sci. **42**, 266-297 (2007).
77. Eslamian, M. Spray-on thin film PV solar cells: advances, potentials and challenges. Coatings **4**, 60-84 (2014).
78. Adelowo, E., Baboukani, A. R., Chen, C. & Wang, C. Electrostatically sprayed reduced graphene oxide-carbon nanotubes electrodes for lithium-ion capacitors. J. Carbon Res. **4**, 31 (2018).
79. Adak, B., Joshi, M. & Butola, B. S. Polyurethane/functionalized-graphene nanocomposite films with enhanced weather resistance and gas barrier properties. Compos. Part B: Eng. **176**, 107303 (2019).

80. Nordin, N. M., Buys, Y. F., Anuar, H., Ani, M. H. & Pang, M. M. Development of conductive polymer composites from pla/tpu blends filled with graphene nanoplatelets. Today Proceeding **17**, 500 (2019).
81. Khanam, P. N. et al. Melt processing and properties of linear low density polyethylene-graphene nanoplatelet composites. Vacuum **130**, 63-71 (2016).
82. Panchakarla, L. S.,Govindaraj, A. & Rao, C. N. R. Nitrogen- and boron-doped double-walled carbon nanotubes. ACS Nano **1**, 494 (2007).
83. Subrahmanyam, K. S., Govindaraj, P. L. & Rao, C. N. R. Simple method of preparing graphene flakes by an arc-discharge method. J. Phys. Chem C **113**, 4257-4259 (2009).
84. Goldberg, D. & Goldberget, D. The tribological properties of solid lubrication graphite coatings prepared by a sol–gel method. Carbon **38**, 2017-2020 (2005).
85. Meyer, J. C., Simon, S.K., Park, J.H., Skakalova, V. & Künze, D. Experimental analysis of charge redistribution due to chemical bonding by high-resolution transmission electron microscopy. Nat. Mater. **10**, 209-215 (2011).
86. Banhart, F., Kotakoski, J. &Krasheninnikov,A. V. Structural defects in graphene. ACS Nano **5**, 26-41 (2011).
87. Ruiz-Vargas, C.S. et al. Softened elastic response and unzipping in chemical vapor deposition graphene membranes. Nano Lett., **11**, 2259-2263 (2011).
88. Stone, A. J. & Wales, D. J. Theoretical studies of icosahedral C_{60} and some related species. Chem. Phys. Lett. **128**,501-503 (1986).
89. Meyer, J. C. et al. Direct imaging of lattice atoms and topological defects in graphene membranes. Nano Lett. **8**, 3582-3586 (2008).
90. Banhart, F., Kotakoski, J. & Krasheninnikov, A. V. Structural defects in graphene. ACS nano **5**, 26-41 (2011).
91. Girit, C.O. et al. Graphene at the edge: stability and dynamics, Science **323**, 1705-1708 (2009).
92. Banhart, F. Interactions between metals and carbon nanotubes: at the interface between old and new materials. Nanoscale **1**, 201-213 (2009).
93. Krasheninnikov, A. & Banhart, F. Engineering of nanostructured carbon materials with electron or ion beams. Nat. Mater. **6**, 723-733 (2007).
94. Tapaszto, L. et al. Tuning the electronic structure of graphene by ion irradiation. Phys. Rev. B **78**, 233407 (2008).
95. Bagri, A. et al. Structural evolution during the reduction of chemically derived graphene oxide. Nat. Chem., **2**, 581-587 (2010).
96. Cortijo, A. & Vozmediano, M.A.H. Effects of topological defects and local curvature on the electronic properties of planar graphene. Nucl. Phys. B **763**, 293-308 (2007).
97. Li, J., Tang, T., Luo, L. & Yao, J. Enhancement and modulation of photonic spin Hall effect by defect modes in photonic crystals with graphene. Carbon **134**, 293-300 (2018).
98. Gouda, M.H. et al. Poly(vinyl alcohol)-based crosslinked ternary polymer blend doped with sulfonated graphene oxide as a sustainable composite membrane for direct borohydride fuel cells. J. Power Sources **432**, 92-101 (2019).
99. Cobos, M., Pinta, I. D. L.,Quindos, G., Fernandeza, M. J. & Fernandeza, M.D. One-step eco-friendly synthesized silver-graphene oxide/poly (vinyl alcohol) antibacterial nanocomposites. Carbon **150**, 101-116 (2019).
100. Feng, L. & Liu, Z. Graphene in biomedicine: opportunities and challenges. Nanomedicine **6,**317-324 (2011).
101. Liu, Z., Robinson, J. T., Tabakman, S. M., Yang, K. &Dai, H. Carbon materials for drug delivery & cancer therapy. Mater. Today **14**, 316-323 (2011).
102. Sharma, B., Shekhar, S., Gautam, S., Sarkar, A. & Jain, P. Nanomechanical analysis of chemically reduced graphene oxide reinforced poly (vinyl alcohol) nanocomposite thin films. Polym. Testing **70**, 458-466 (2018)
103. Malik, P., Bhasha, B. & Jain, P. Influence of surface modified graphene oxide on mechanical and thermal properties of epoxy resin. Orient J. Chem. **34**, 1597-1603 (2018).
104. Wang, Z. et al. Ultrahigh dielectric constant and low loss of highly-aligned graphene aerogel/poly (vinyl alcohol) composites with insulating barriers. Carbon **123**, 385-394 (2017).

105. Khan, A., Jain, R. K., Luqman, M. & Asiri,A. M. Development of sulfonated poly (vinyl alcohol)/aluminium oxide/graphene based ionic polymer-metal composite (IPMC) actuator. Sens. Actuator A Phys. **280**, 114-124 (2018).
106. Huang, Y., Liang, J. &Chen, Y. The application of graphene based materials for actuators. J. Mater. Chem. **22**, 3671-3679 (2012).
107. Chattaraj, R., Bhaumik, S., Khan, S. &Chatterjee, D. Soft wearable ionic polymer sensors for palpatory pulse-rate extraction. Sens. Actuators A: Phys. **270**, 65-71 (2018).
108. Dong, J., Wang, Z. & X. Kang. The synthesis of graphene/PVDF composite binder and its application in high performance MnO_2 supercapacitors. Colloids and Surfaces A: Physicochem. Eng. Aspects **489**, 282–288 (2016).
109. Ahmad, A. L., Farooqui, U. R. & Hamid, N. A. Synthesis and characterization of porous poly(vinylidene fluoride-co-hexafluoro propylene) (PVDF-co-HFP)/poly(aniline) (PANI)/graphene oxide (GO) ternary hybrid polymer electrolyte membrane. Electrochim. Acta **283**, 842-849(2018).
110. Wan, Y. J., Yang, W. H., Yu, S. H., Sun, R., Wong, C. P. & Liao, W. H. Covalent polymer functionalization of graphene for improved dielectric properties and thermal stability of epoxy composites. Compos. Sci. Technol. **122**, 27-35 (2016).
111. Moharana, S. & Mahaling, R.N. Silver (Ag)-Graphene oxide (GO) - Poly (vinylidene fluoride-co-hexafluoropropylene) (PVDF-HFP) nanostructured composites with high dielectric constant and low dielectric loss. Chem. Phys. Lett. **680**, 31-36 (2017).
112. Chen, Z., Liu, Y., Fang, L., Jiang, P. & Huang, X. Role of reduced graphene oxide in dielectric enhancement of ferroelectric polymers composites. Appl. Surf. Sci. **470**, 348-359 (2019).
113. He, Z. Z. et al. Compos. Part ALargely enhanced dielectric properties of poly (vinylidene fluoride) composites achieved by adding polypyrrole-decorated graphene oxide. Appl. Sci. Manuf. **104**, 89–100 (2018).
114. Li, Y. et al. Fe_3O_4 decorated graphene/poly (vinylidene fluoride) nanocomposites with high dielectric constant and low dielectric loss. Compos. Sci. Technol. **171**, 152-161 (2019).
115. Li, Y. et al. Polydopamine coating layer on graphene for suppressing loss tangent and enhancing dielectric constant of poly (vinylidene fluoride)/graphene composites. Compos. Part A Appl. Sci. Manuf. **73**, 85-92 (2015).
116. Zhang, Y., Wang, Y., Deng, Y., Li, M. & Bai, J. Enhanced dielectric properties of ferroelectric polymer composites induced by metal-semiconductor Zn-ZnO core–shell structure. ACS Appl. Mater. Interfaces **4**, 65-68 (2012).
117. Tong, W. et al. Amorphous TiO_2-coated reduced graphene oxide hybrid nanostructures for polymer composites with low dielectric loss. Chem. Phys. Lett. **638**, 43-46 (2015).
118. Tong, W. et al. Achieving significantly enhanced dielectric performance of reduced graphene oxide/polymer composite by covalent modification of graphene oxide surface. Carbon **94**, 590-598 (2015).
119. Li, H. et al. Poly (vinyl pyrrolidone)-coated graphene/poly (vinylidene fluoride) composite films with high dielectric permittivity and low loss. Compos. Sci. Technol.**121**, 49-55 (2015).
120. Wu, Y. et al. Exceptional dielectric properties of chlorine-doped graphene oxide/poly (vinylidene fluoride) nanocomposites. Carbon **89**, 102-112 (2015).
121. Gangineni,P. K. Mechanical behavior of Graphene decorated carbon fiber reinforced polymer composites: An assessment of the influence of functional groups. Compos. Part A: Appl. Sci. Manuf. **122**, 36-44 (2019).
122. Wan, Y. J. et al. Grafting of epoxy chains onto graphene oxide for epoxy composites with improved mechanical and thermal properties. Carbon **69**, 467-480 (2014).
123. Surnova, A., Balkaev, D., Musin, D. Amirov, R. & Dimiev, A. M. Fully exfoliated graphene oxide accelerates epoxy resin curing, and results in dramatic improvement of the polymer mechanical properties. Compos. Part B. Eng. **162**, 685-691 (2019).
124. Feng, Y. et al. Multiple synergistic effects of graphene-based hybrid and hexagonal born nitride in enhancing thermal conductivity and flame retardancy of epoxy. Chem. Eng. J. **379**, 122402 (2020).

125. Gong, X. et al. Amino graphene oxide/dopamine modified aramid fibers: Preparation, epoxy nanocomposites and property analysis. Polym. **168**, 131-137 (2019).
126. Zhang, T. et al. Grafting of polystyrene onto reduced graphene oxide by emulsion polymerization for dielectric polymer composites: High dielectric constant and low dielectric loss tuned by varied grafting amount of polystyrene. Eur. Polym. J. **94**, 196-207 (2017).
127. Liu, Y. et al. Polystyrene/graphene oxide nanocomposites synthesized via Pickering polymerization. Prog. Org. Coat. **99**, 23-31 (2016).
128. He, F. et al. Fabrication of graphene nanosheet (GNS)–Fe_3O_4 hybrids and GNS–Fe_3O_4/syndiotactic polystyrene composites with high dielectric permittivity. Carbon **58**, 175 (2 013)
129. Tu, Z. et al. A facile approach for preparation of polystyrene/graphene nanocomposites with ultra-low percolation threshold through an electrostatic assembly process. Compos. Sci. Technol. **134**, 49-56 (2016).
130. Chen, Y. et al. Enhanced electromagnetic interference shielding efficiency of polystyrene/graphene composites with magnetic Fe_3O_4 nanoparticles. Carbon **82**, 67-76 (2015).
131. Wang, J., Jin, X., Zhang, X., Wu, H. & Guo, S. Effect of tunable styrene content on achieving high-performance poly (styrene-b-ethylene-ran-butylene-b-styrene)/graphene oxide nanocomposites. Compos. Sci. Technol. **164**, 229-237 (2018).
132. Deshmukh, K. et al.Graphene oxide reinforced poly (4-styrenesulfonic acid)/polyvinyl alcohol blend composites with enhanced dielectric properties for portable and flexible electronics. Mater. Chem.Phys. **186**, 188-201 (2017).
133. Adloo, A., Sadeghi, M., Masoomi, M. & Pazhooh, H. N. High performance polymeric bipolar plate based on polypropylene/graphite/graphene/nano-carbon black composites for PEM fuel cells. Renew. Energy **99**, 867-874 (2016).
134. Wang, D. et al. Dielectric properties of reduced graphene oxide/polypropylene composites with ultralow percolation threshold. Polym. **54**, 1916-1922 (2013).
135. Cao, L., Su, D., Su, Z. & Chen, X. Fabrication of multiwalled carbon nanotube/polypropylene conductive fibrous membranes by melt electrospinning. Ind. Eng. Chem. Res. **53**, 2308-2317 (2014).
136. Song, N. et al. Highly thermally conductive polypropylene/graphene composites for thermal management. Compos. Part A: Appl. Sci. Manufact. **135**, 105912 (2020).
137. Bafana, A.P. et al., Polypropylene nanocomposites reinforced with low weight percent graphene nanoplatelets. Compos. Part B: Eng. **109**, 101-107 (2017).
138. Song, P. et al. Fabrication of exfoliated graphene-based polypropylene nanocomposites with enhanced mechanical and thermal properties. Polym. **52**, 4001-4010 (2011).
139. Chen, M. et al. Dielectric and mechanical properties and thermal stability of polyimide–graphene oxide composite films. Thin Solid Films **584**, 232-237 (2015).
140. Luong, N. D. et al. Enhanced mechanical and electrical properties of polyimide film by graphene sheets via in situ polymerization, Polym. **52**, 5237-5242 (2011).
141. Ramakrishnan, S., Dhakshnamoorthy, M., Jelmy, E. J., Vasanthakumari, R. & Kothurkar, N. K. Synthesis and characterization of graphene oxide–polyimide nanofiber composites. RSC Adv. **4**, 9743-9749 (2014).
142. Yi, B., Zhao, Y., Tian, E., Li, J. & Ren, Y. High-performance polyimide nanofiber membranes prepared by electrospinning. High Performance Polym. **31**, 438-448 (2019).
143. Pokharel, P. et al. Effects of functional groups on the graphene sheet for improving the thermomechanical properties of polyurethane nanocomposites. Compos. Part B **78**, 192-201 (2015).
144. Yuan, Z., Lu, Z., Yang, Z., Sun, J. & Xie, F. A criterion for the normal properties of graphene/polymer interface. Comput. Mater. Sci. **120**, 13-20 (2016).
145. Jiang, L.Y. et al. A cohesive law for carbon nanotube/polymer interfaces based on the van der Waals force. J. Mech. Phys. Solids **54**, 2436-2452 (2006).
146. Sadasivuni, K. K. et al. Dielectric properties of modified graphene oxide filled polyurethane nanocomposites and its correlation with rheology. Compos. Sci. Technol. **104**, 18-25 (2014).

147. Gupta, S., McDonald, B., Carrizosa, S. B. & Price, C. Microstructure, residual stress, and intermolecular force distribution maps of graphene/polymer hybrid composites: Nanoscale morphology-promoted synergistic effects. Compos. Part B: Eng. **92**, 175-192 (2016).
148. Du, Y. et al. Simultaneous increase in conductivity and Seebeck coefficient in a polyaniline/graphene nanosheets thermoelectric nanocomposite. Synt. Met. **161**, 2688 -2692 (2012).
149. Haldar, P., Biswas, S., Sharma, V., Chowdhury, A. & Chandra, A. Mn_3O_4-polyaniline-graphene as distinctive composite for use in high-performance supercapacitors. Appl. Surf. Sci. **491**, 171-179 (2019).
150. Gómez, H. et al. Graphene-conducting polymer nanocomposite as novel electrode for supercapacitors. J. Power Sources, **196**, 4102-4108 (2011).
151. Wang, H., Hao, Q., Yang, X., Lu, L. & Wang, X. Graphene Oxide Doped Polyaniline for Supercapacitors. Electrochem. commun. **11**, 1158-1161(2009).
152. Jin, Y., Huang, S., Zhang, M. & Jia, M. Preparation of sulfonated graphene–polyaniline nanofiber composites by oil/water interfacial polymerization and their application for supercapacitors. Synth. Met., **168**, 58-64 (2013).
153. Ansari, M.O. et al. pTSA doped conducting graphene/polyaniline nanocomposite fibers: Thermoelectric behavior and electrode analysis. Chem. Eng. J. **242**, 155-161 (2014).
154. Luo, Y. et al. Electricity generation from indole and microbial community analysis in the microbial fuel cell. J. Hazard Mater. **176**, 759-764 (2010).
155. Liu, Y. et al. Graphene/polypyrrole intercalating nanocomposites as supercapacitors electrode Electrochim. Acta **112**, 44-52 (2013).
156. Li, S. et al. One-step synthesis of graphene/polypyrrole nanofiber composites as cathode material for a biocompatible zinc/polymer battery. ACS Appl. Mater. Interfaces **6**, 16679-16686 (2014).
157. Ding, X., Spinning fabrication of graphene/polypyrrole composite fibers for all-solid-state, flexible fibriform supercapacitors. J. Mater. Chem. A **2**, 12355-12360 (2014).
158. Li, Y. et al. Remarkably enhanced performances of novel polythiophene-grafting-graphene oxide composite via long alkoxy linkage for supercapacitor application. Carbon, **147**, 519-531 (2019).
159. Nayebi, P. & Zaminpayma, E. A molecular dynamic simulation study of mechanical properties of graphene–polythiophene composite with Reax force field. Phys. Lett. A **380**, 628-633 (2016).
160. Iguchi, H. Et al. Preparation of uncurled and planar multilayered graphene using polythiophene derivatives via liquid-phase exfoliation of graphite. Flat Chem. **8**, 31-39 (2018).
161. Alabadi, A., Razzaque, S., Dong, Z., Wang, W. & Tan, B. Graphene oxide-polythiophene derivative hybrid nanosheet for enhancing performance of supercapacitor. J. Power Sources **306**, 241-247 (2016).